SUPPORTING INFORMATION

Ruthenium molecular complexes immobilized on graphene as active catalysts for the synthesis of carboxylic acids from alcohol dehydrogenation

David Ventura-Espinosa,[a] Cristian Vicent,[b] Miguel Baya[c] and Jose A. Mata[a,]*

[a]Institute of Advanced Materials (INAM), Universitat Jaume I, Avda. Sos Baynat s/n, 12006, Castellón (Spain) E-mail: jmata@uji.es Fax: (+34) 964387522; Tel: (+34) 964387516
[b]Serveis Centrals d'Intrumentació Científica (SCIC). Universitat Jaume I, Avda. Sos Baynat s/n, 12071, Castellón (Spain)
[c]Instituto de Síntesis Química y Catálisis Homogénea (ISQCH), Departamento de Química Inorgánica, CSIC-Universidad de Zaragoza, C/Pedro Cerbuna 12, E-50009 Zaragoza (Spain)

Contents

1. Experimental section

General procedures

Anhydrous solvents were dried using a solvent purification system (SPS M BRAUN) and used for the synthesis of the imidazolium salts. Regular solvents were used for the synthesis of ruthenium complexes hybrid materials. Milli-Q water was used for the catalytic experiments. Graphite powder (natural, universal grade, 200 mesh, 99.9995 %) and all other reagents were used as received from commercial suppliers. Graphene oxide, reduced graphene oxide, $[RuCl_2(p\text{-cymene})]_2$ complex **3** and imidazolium salts **PhF**, **Ant** and **Pyr** were obtained according to the known published methods.

Preparation of metal complexes

Synthesis of PhF-Ru (1). Silver oxide (102 mg, 0.44 mmol) was added to a solution of 1 - pentafluorobenzyl - 3 - methylimidazolium bromide (248 mg, 0.72 mmol) in CH_2Cl_2 in a round bottom flask covered with aluminium foil. The suspension was stirred at room temperature for 1 h. Then $[Ru(p\text{-cymene})Cl_2]_2$ (200 mg, 0.32 mmol) was added to the suspension and stirred overnight at reflux temperature. After solvent removal, the crude product was purified by column chromatography. The pure compound **1** was eluted with dichloromethane/acetone (9:1). After solvent removal, compound **1** was obtained as an orange solid. Yield: 120 mg (33 %)

Synthesis of Ant-Ru (2). Silver oxide (102 mg, 0.44 mmol) was added to a solution of 1 - (9 - methylantracene) - 3- methylimidazolium chloride (223 mg, 0.72 mmol) in CH_2Cl_2 in a round bottom flask covered with aluminium foil. The suspension was stirred at room temperature for 1 h. Then $[Ru(p\text{-cymene})Cl_2]_2$ (200 mg, 0.32 mmol) was added to the suspension and stirred overnight at reflux temperature. After solvent removal, the crude product was purified by column chromatography. The pure compound **2** was eluted with dichloromethane/acetone (95:5). Recrystallization from a dichloromethane/hexane mixture afforded compound **2** as an orange solid. Yield: 170 mg (46 %).

General procedure for the preparation of M-rGO materials

In a round-bottom flask were introduced 90 mg of rGO and 10 mL of dichloromethane. The suspension was sonicated for 30 minutes. Then, 10 mg of the corresponding metal complex **1** - **3** was added to the suspension. The mixture was stirred at room temperature for 10 hours. The black solid was filtered off and washed with 2 x 15 mL of dichloromethane. The filtrates were combined and evaporated to dryness under reduced pressure. The presence of unsupported complex **1 - 3** were analyzed by ^1H NMR using anisole as internal standard. Integration of the characteristic signal of anisole (-O*Me*) vs. (NCH_3) accounts for a first indication of the complex amount deposited onto rGO. The exact amount of complex supported was determined by ICP-MS analysis. Digestion of the materials was performed in a refluxing mixture of nitric and hydrochloric acids (3:1) for 12h.

General procedure for catalytic experiments

Catalytic assays were performed in a round bottom flask, using 1 equivalent of alcohol, 1 equivalent of cesium carbonate, catalyst and 10 mL of solvent for 24 hours at 100 °C. Yields and conversions were determined by GC analysis using anisole as external standard. Isolated yields were determined by ^{1}H NMR using an appropriate external standard depending of the product analysed.

Recycling experiments were carried out under the same reaction conditions as described before. After completion of each run (24 h), the reaction mixture was allowed to reach room temperature and the catalyst was isolated by decantation. The remaining solid was washed thoroughly with water and reused in the following run.

Procedure for hydrogen identification

All glassware was carefully clean and rinsed with Milli-Q water prior to use. A 25 mL round bottom flask was charged with 0.44 mmol of 4-methyl benzyl alcohol, 0.44 mmol of cesium carbonate, $8.8 \cdot 10^{-3}$ mmol of catalyst **PhF-Ru (1)** and 10 mL of water and heated at 100 ^{o}C. At selected times, a 1.5 mL sample of the generated gas was collected and the hydrogen content was qualitative analysed by gas chromatography (GS-MOL 15 meters column ID 0.55 mm TCD from J&W Scientific).

2. High Resolution Mass Spectroscopy (HRMS)

Mass spectra were obtained using a QTOF Premier (quadrupole-hexapole-TOF) with an orthogonal Z-spray-electrospray interface (Waters, Manchester, UK). The drying gas as well as nebulizing gas was nitrogen at a flow of 400L/h and 80 L/h respectively. The temperature of the source block was set to 120 ^{o}C and the desolvation temperature to 150 ^{o}C. A capillary voltage of 3.5 KV was used in the positive scan mode and the cone voltage was set to 10 V to control the extent of fragmentation. Mass calibration was performed using a solution of sodium iodide in isopropanol:water (50:50) from m/z 150 to 1000 Da. Sample solutions (ca. 1×10^{-5} M) were infused via syringe pump directly connected to the interface at a flow of 10 μl/min. A 1 μg/mL solution of Luekine-enkephaline was used as lock mass for accurate m/z determinations.

2.1 HRMS of complex **PhF-Ru (1)**

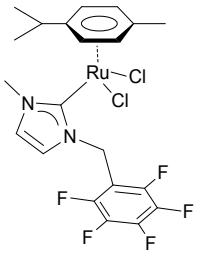

MW: 567,92 g/mol

Fragment: 533,03 $[M-Cl]^+$

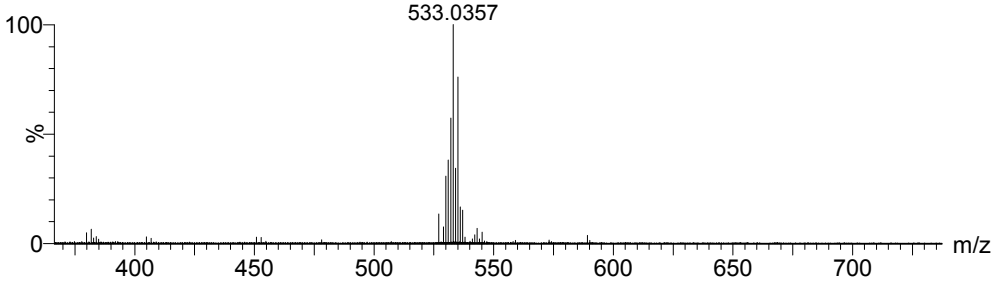

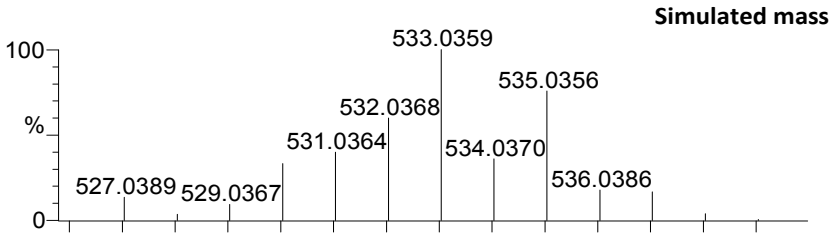

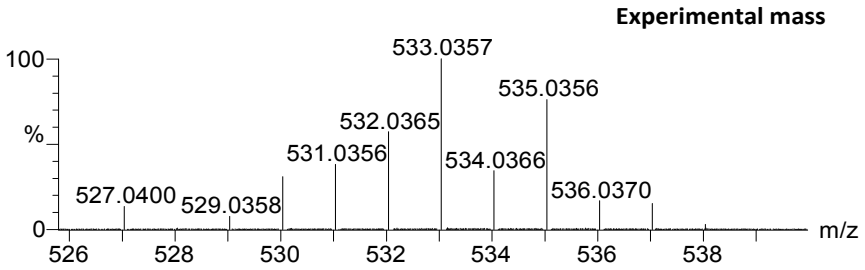

Peak (m/z)	Experimental mass	Simulated mass	Relative error (ppm)
533.03	533.0357	533.0359	0.4

2.2 HRMS of compound **Ant-Ru (2)**

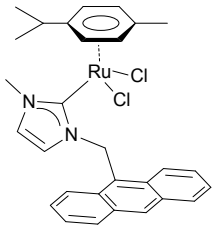

MW: 578,92 g/mol

Fragment: 543,11 $[M-Cl]^+$

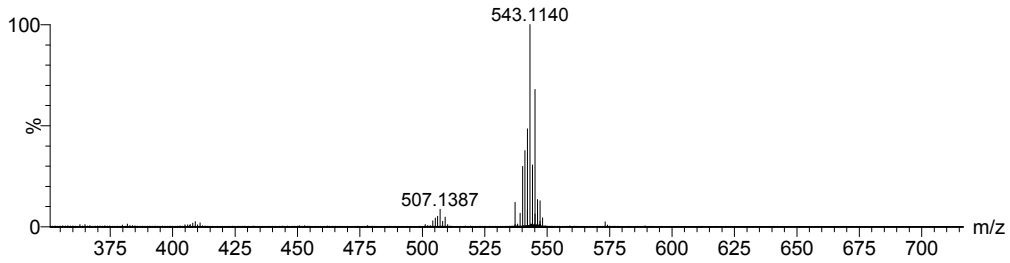

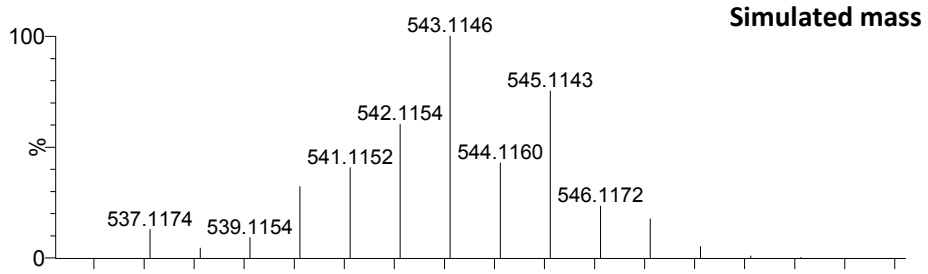

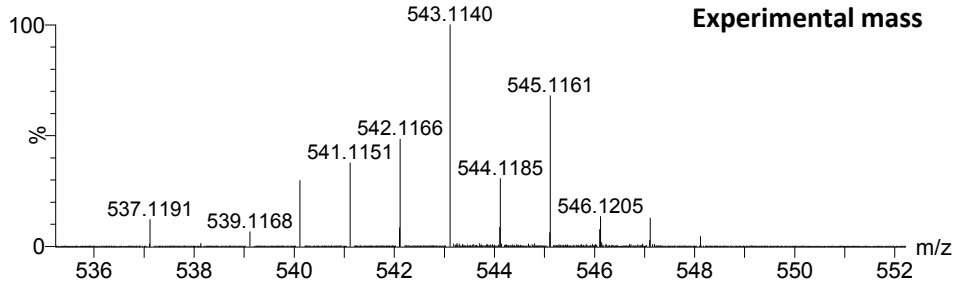

Peak (m/z)	Experimental mass	Simulated mass	Relative error (ppm)
543.11	543.1140	543.1146	1.6

3. Nuclear Magnetic Resonance (NMR) Analysis

NMR spectra were recorded on Varian spectrometers operating at 300 or 500 MHz (^{1}H NMR) and 75 and 125 MHz (^{13}C{^{1}H} NMR), respectively, and referenced to $SiMe_4$ (δ in ppm and J in Hertz). NMR spectra were recorded at room temperature with the appropriate deuterated solvent.

3.1 NMR spectra of complex **PhF-Ru (1)**

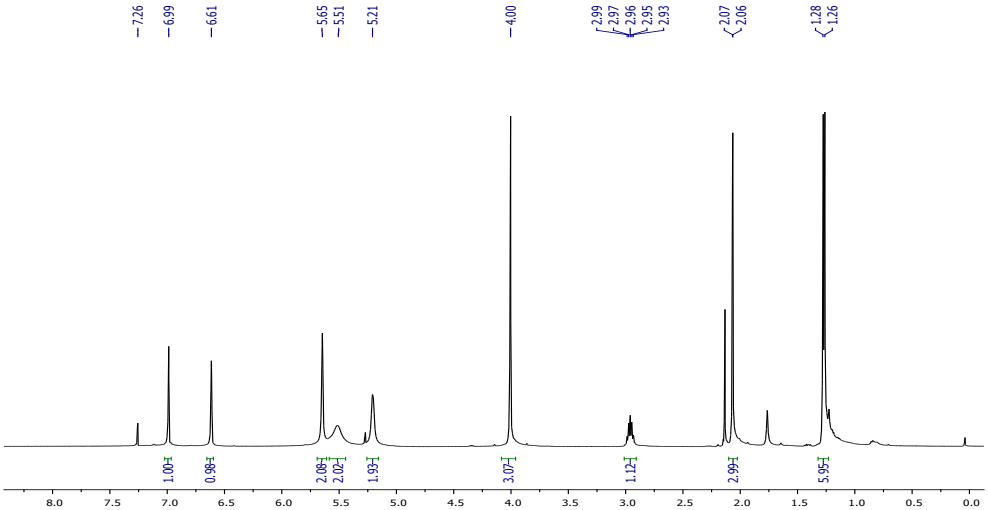

^{1}H NMR (500 MHz, $CDCl_3$): δ 6.99 (s, 1H, C*H*$_{imid}$), 6.61 (s, 1H, C*H*$_{imid}$), 5.65 (s, 2H, NC*H*$_2$-), 5.51 (s, 2H, C*H*$_{p\text{-}cym}$), 5.21 (s, 2H, C*H*$_{p\text{-}cym}$), 4.00 (s, 3H, NC*H*$_3$), 2.96 (m, 1H, C*H*$_{iPr,\ p\text{-}cym}$), 2.07 (s, 3H, C*H*$_{3,p\text{-}cym}$) 1.27 (d, $^3J_{H\text{-}H}$ = 6.9 Hz, 6H, C*H*$_{3,iPr\ p\text{-}cym}$).

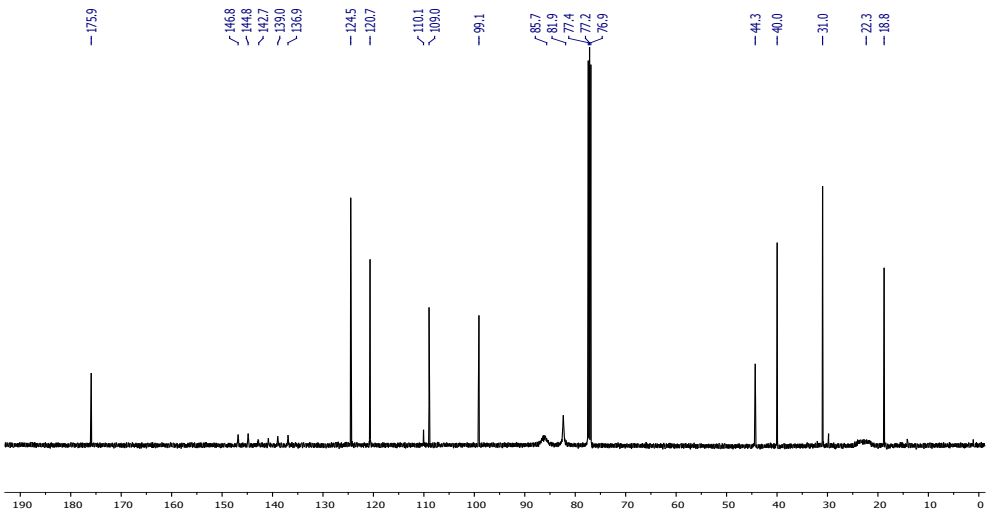

^{13}C{^{1}H} NMR (125 MHz, $CDCl_3$): δ 175.9 ($C_{carbene}$-Ru), [146.8, 144.8, 142.7, 140.9, 139.0, 136.9] (C-F), [124.5, 120.7] (CH_{imid}), [109.0, 99.1] ($Cq_{p\text{-}cym}$), [85.7, 81.9] ($CH_{p\text{-}cym}$), 44.3 (N-CH_2-), 40.0 (NCH_3), 31.0 ($CH_{iPr,\ p\text{-}cym}$), 22.3 ($CH_{3,\ p\text{-}cym}$), 18.8 ($CH_{3,\ iPr\ p\text{-}cym}$).

3.2 NMR spectra of complex **Ant-Ru (2)**

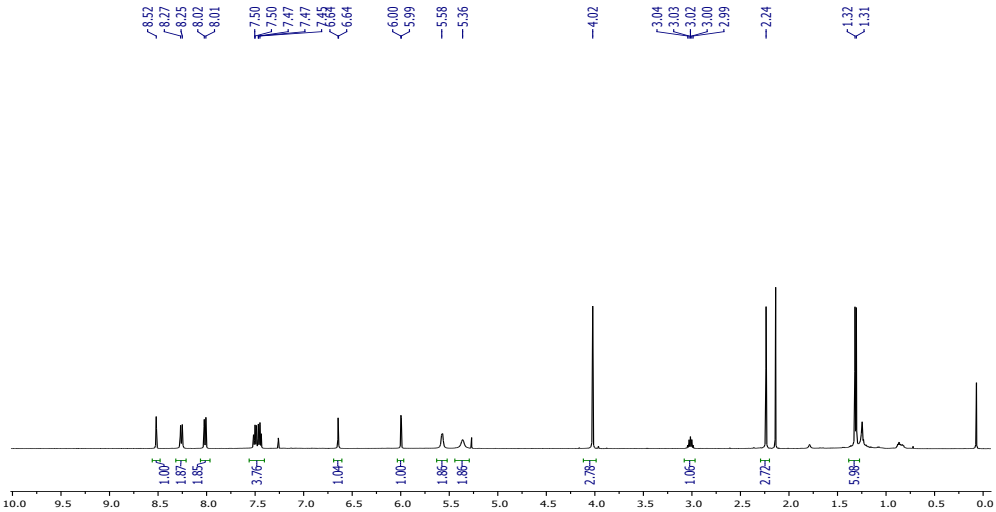

^{1}H NMR (500 MHz, $CDCl_3$): δ 8.52 (s, 1H, C*H*$_{ant}$), 8.26 (d, $^{3}J^{H-H}$ = 8.7 Hz, 2H, C*H*$_{ant}$), 8.02 (d, $^{3}J_{H-H}$ = 8.2 Hz, 2H, C*H*$_{ant}$), 7,56 – 7,40 (m, 4H, C*H*$_{ant}$), 6.64 (d, $^{3}J_{H-H}$ = 2.0 Hz, 1H, C*H*$_{imid}$), 6.00 (d, $^{3}J_{H-H}$ = 1.9 Hz, 1H, C*H*$_{imid}$), 5.58 (s, 2H, C*H*$_{p\text{-}cym}$), 5.36 (s, 2H, C*H*$_{p\text{-}cym}$), 4.02 (s, 3H, NC*H*$_3$), 3.02 (m, 1H, C*H*$_{iPr,\ p\text{-}cym}$), 2.24 (s, 3H, C*H*$_{3,\ p\text{-}cym}$), 1.31 (d, $^{3}J_{H-H}$ = 6.9 Hz, 6H, C*H*$_{3,iPr\ p\text{-}cym}$).

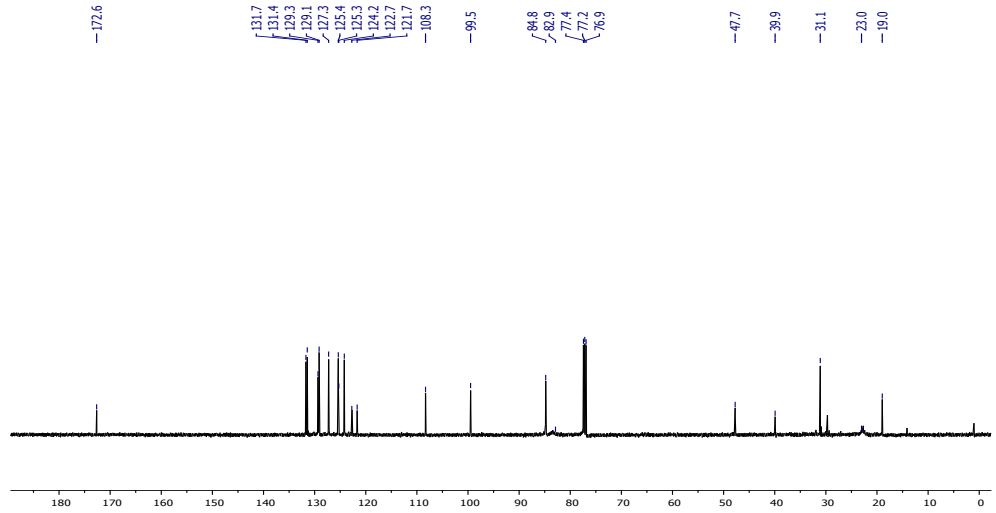

^{13}C{^{1}H} NMR (125 MHz, C_6D_6): δ 172.6 ($C_{carbene}$-Ru), [131.7, 131.4, 129.3, 129.1, 127.3, 125.4, 125.3, 124.2, 122.7, 121.7] (C_{ant}, CH_{imid}), [108.3, 99.5] ($Cq_{p\text{-}cym}$), [84.8, 82.9] ($CH_{p\text{-}cym}$), 47.7 (N-CH_2-), 39.9 (NCH_3), 31.1 ($CH_{iPr,\ p\text{-}cym}$), 23.0 ($CH_{3,\ p\text{-}cym}$), 19.0 ($CH_{3,\ iPr\ p\text{-}cym}$).

4. X-Ray Diffraction Studies

Crystallographic data and structure refinement for compound PhF-Ru (**1**).

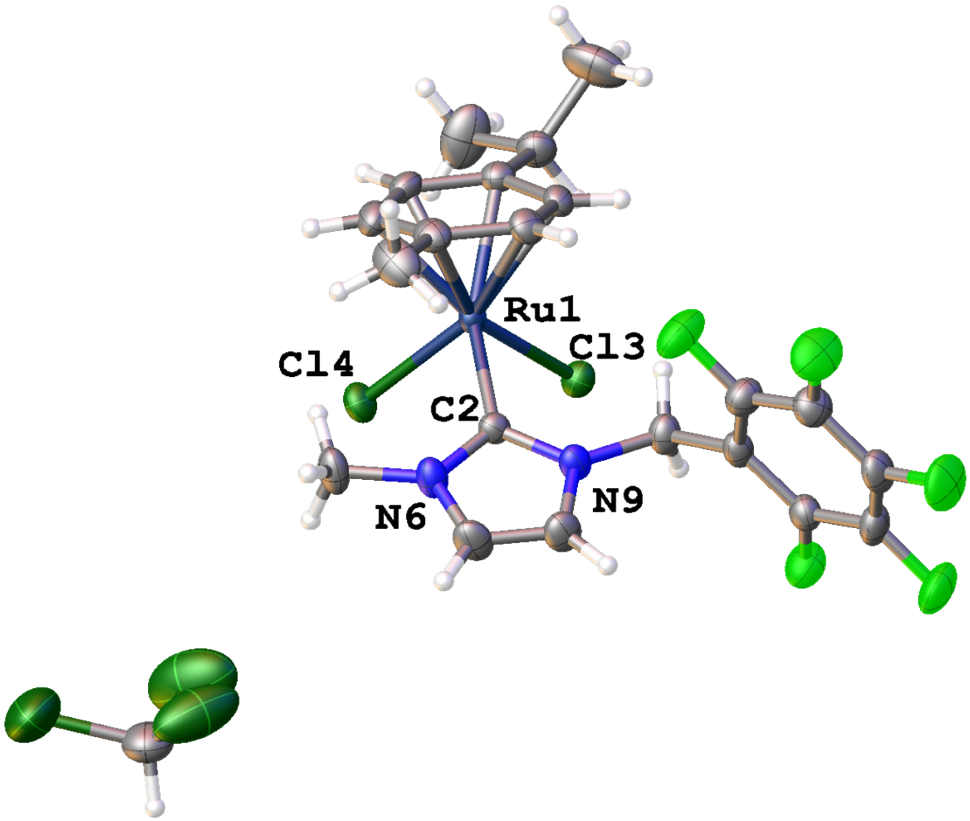

Molecular diagram of compound PhF-Ru (**1**). Ellipsoids are at 50% probability level. Hydrogen atoms omitted for clarity. Selected bond lengths [Å] and angles [º]: Ru(1) - C(2) 2.065(3), Ru(1) - Cl(3) 2.4229(7), Ru(1) - Cl(4) 2.4205(7), Ru(1) - Ph_{cent} 1.69, C(2) - N(6) 1.360(3), C(2) - N(9) 1.365(3), Cl(3) - Ru(1) - Cl(4) 84.65(2), C(2) - Ru(1) - Cl(3) 89.81(8), C(2) - Ru(1) - Cl(4) 90.05(7), N(6) - C(2) - N(9) 103.3(2).

Table S1 Crystal data and structure refinement for PhF-Ru (**1**).

Identification code	str1733
Empirical formula	$C_{22}H_{22}Cl_5F_5N_2Ru$
Formula weight	687.74
Temperature/K	293(2)
Crystal system	monoclinic
Space group	$P2_1/c$
a/Å	15.9690(4)
b/Å	10.6225(4)
c/Å	15.6395(5)
α/°	90.00
β/°	91.922(3)
γ/°	90.00
Volume/Å^3	2651.44(15)
Z	4
ρ_{calc}g/cm^3	1.723
μ/mm^{-1}	1.146
F(000)	1368.0
Crystal size/mm^3	0.11 × 0.1 × 0.09
Radiation	MoKα (λ = 0.71073)
2Θ range for data collection/°	5.72 to 58.92
Index ranges	$-22 \leq h \leq 22$, $-14 \leq k \leq 13$, $-21 \leq l \leq 20$
Reflections collected	29917
Independent reflections	6622 [R_{int} = 0.0518, R_{sigma} = 0.0391]
Data/restraints/parameters	6622/0/347
Goodness-of-fit on F^2	0.859
Final R indexes [I>=2σ (I)]	R_1 = 0.0351, wR_2 = 0.0833
Final R indexes [all data]	R_1 = 0.0463, wR_2 = 0.0997
Largest diff. peak/hole / e Å^{-3}	0.56/-1.02

Table S2 Fractional Atomic Coordinates ($\times 10^4$) and Equivalent Isotropic Displacement Parameters ($Å^2 \times 10^3$) for PhF-Ru (**1**). U_{eq} is defined as 1/3 of of the trace of the orthogonalised U_{IJ} tensor.

Atom	*x*	*y*	*z*	U(eq)
Ru1	2969.21(12)	5318.8(2)	5269.82(13)	22.19(7)
Cl33	6310(4)	10403(6)	3949(4)	75.0(12)
Cl4	4058.1(4)	6503.4(7)	4590.7(4)	31.66(15)
Cl3	2042.7(4)	6939.5(7)	4695.7(4)	28.62(14)
Cl34	5983(4)	9680(7)	5662(5)	85.5(15)
Cl32	7673(4)	9589(7)	5057(7)	130(4)
F13	721.7(12)	9066.8(19)	7174.6(13)	45.4(5)
F19	505.8(16)	4930(2)	9170.1(14)	57.8(6)
F15	-223.2(13)	9116(2)	8559.0(14)	55.5(6)
F21	1494.1(15)	4894(2)	7805.1(13)	53.1(5)
F17	-348.1(13)	7049(2)	9555.8(13)	58.7(6)
C22	3781(2)	3362(4)	6795(2)	48.9(9)
C30	1087(3)	3153(5)	3517(3)	70.4(13)
C14	194.0(18)	8065(3)	8365(2)	36.7(7)
C31	2298(3)	4109(5)	2777(2)	66.4(12)
C11	1143.8(16)	6981(3)	7451.7(17)	29.2(6)
C2AA	6725(3)	10373(4)	4974(3)	59.1(10)
C23	3276.6(18)	3576(3)	5975(2)	32.8(6)
C12	693.8(17)	8034(3)	7663.0(18)	30.5(6)
N6	3888.6(14)	6588(3)	6815.2(15)	32.0(5)
C29	1796.5(19)	4101(3)	3582(2)	36.8(7)
N9	2568.7(14)	6877(2)	6882.4(14)	27.8(5)
C20	1070.1(19)	5950(3)	7980(2)	35.8(6)
C10	1665.2(17)	6934(3)	6663.7(18)	31.9(6)
C18	570(2)	5948(3)	8684(2)	38.1(7)
C5	4731.1(17)	6258(4)	6561(2)	40.7(8)
C2	3156.2(16)	6365(3)	6372.6(16)	24.6(5)
C16	133.6(18)	7021(3)	8868(2)	38.6(7)
C25	1945.2(16)	3999(3)	5207.3(18)	27.7(5)
C8	2931.4(19)	7406(3)	7614.5(18)	36.6(7)
C28	3662.6(18)	3563(3)	5180(2)	33.9(6)
C27	3185.7(17)	3680(3)	4403.4(19)	30.4(6)
C26	2327.0(17)	3888(3)	4392.5(18)	29.3(6)
C7	3755.9(19)	7215(3)	7569.8(19)	38.9(7)
C24	2399.8(18)	3806(3)	5979.7(19)	31.8(6)
Cl	7678(5)	9680(9)	4731(6)	120(3)
Cl1	6062(5)	10183(8)	4093(5)	135(3)
Cl2	6359(5)	9646(7)	5840(5)	115(3)

Table S3 Anisotropic Displacement Parameters ($Å^2 \times 10^3$) for PhF-Ru (**1**). The Anisotropic displacement factor exponent takes the form: $-2\pi^2[h^2a^{*2}U_{11}+2hka^*b^*U_{12}+\ldots]$.

Atom	U_{11}	U_{22}	U_{33}	U_{23}	U_{13}	U_{12}
Ru1	19.76(11)	25.74(13)	21.25(12)	-0.61(7)	3.29(8)	-0.07(7)
Cl33	104(3)	64.5(19)	57.9(16)	-1.4(13)	25.2(18)	3.9(17)
Cl4	25.8(3)	38.5(4)	30.9(3)	5.3(3)	5.7(2)	-3.8(3)
Cl3	29.3(3)	31.1(3)	25.4(3)	1.0(2)	0.7(2)	3.7(3)
Cl34	107(3)	73(2)	79(3)	11.7(18)	26(2)	-22(2)
Cl32	68(3)	49(2)	269(10)	6(4)	-58(5)	8(2)
F13	46.5(10)	40.7(11)	49.6(11)	7.0(9)	12.2(9)	8.1(9)
F19	74.5(15)	53.5(13)	46.9(12)	15.1(10)	22.6(11)	1.2(12)
F15	51.8(12)	52.9(13)	63.2(13)	-5.2(11)	24.6(10)	18.9(10)
F21	72.2(14)	40.8(11)	47.7(12)	3.8(9)	24(1)	18.1(10)
F17	56.5(12)	73.8(16)	48.0(12)	0.2(11)	32.7(10)	5.4(11)
C22	46.7(18)	50(2)	50(2)	20.4(17)	-11.8(16)	0.4(16)
C30	78(3)	66(3)	65(3)	1(2)	-28(2)	-31(2)
C14	27.0(13)	46.3(18)	37.2(16)	-8.5(14)	8.0(12)	5.2(13)
C31	69(3)	99(4)	30.9(18)	-3(2)	3.2(17)	22(3)
C11	23.5(12)	39.3(16)	25.1(13)	-6.5(11)	4(1)	-2.4(11)
C2AA	65(3)	38(2)	75(3)	-2.5(18)	5(2)	-3.8(18)
C23	34.2(14)	26.0(14)	38.0(16)	4.4(12)	-1.0(12)	-1.3(12)
C12	24.4(12)	35.0(15)	32.2(14)	-1.6(12)	1.8(11)	-0.8(11)
N6	24.1(11)	46.8(15)	25.0(11)	-3.5(10)	1.9(9)	-1.7(10)
C29	37.3(15)	39.5(17)	33.4(15)	-7.2(13)	-1.0(12)	-2.3(13)
N9	26(1)	36.4(13)	21.2(11)	-4.7(9)	4.0(8)	-2.4(9)
C20	37.7(15)	35.6(17)	34.6(15)	-3.4(13)	7.9(12)	2.6(13)
C10	27.0(13)	42.7(17)	26.2(13)	-2.4(12)	3.5(10)	2.9(12)
C18	39.5(15)	42.5(18)	32.7(15)	0.4(13)	8.1(13)	-3.3(14)
C5	22.0(12)	63(2)	36.5(16)	-7.3(15)	0.0(11)	-0.4(14)
C2	25.4(12)	27.1(13)	21.6(12)	-2.8(10)	4.1(9)	-3.1(10)
C16	29.4(14)	54(2)	33.6(15)	-6.7(14)	12.2(12)	-4.1(14)
C25	22.9(12)	25.5(13)	35.1(14)	-0.3(11)	5.7(10)	-4.2(10)
C8	36.2(15)	47.6(19)	26.2(14)	-9.2(13)	7.0(12)	-2.2(14)
C28	27.6(13)	26.3(14)	48.2(17)	-0.4(12)	6.8(12)	3.9(11)
C27	32.3(13)	24.7(14)	34.9(15)	-6.2(11)	8.6(11)	1.5(11)
C26	30.8(13)	24.5(13)	32.7(14)	-2.6(11)	2.9(11)	-2.0(11)
C7	35.7(15)	55(2)	25.7(14)	-12.5(13)	0.2(12)	-8.9(14)
C24	32.0(13)	31.7(15)	32.3(14)	2.5(12)	8.3(11)	-5.8(12)
Cl	92(4)	78(4)	193(7)	-48(4)	42(4)	7(3)
Cl1	173(7)	112(5)	115(5)	-20(4)	-64(4)	26(4)
Cl2	208(8)	61(2)	79(3)	-2(2)	50(4)	7(4)

Table S4 Bond Lengths for PhF-Ru (**1**).

Atom	Atom	Length/Å	Atom	Atom	Length/Å
Ru1	Cl4	2.4205(7)	C11	C12	1.376(4)
Ru1	Cl3	2.4229(7)	C11	C20	1.380(4)
Ru1	C23	2.202(3)	C11	C10	1.511(4)

Ru1	C2	2.065(3)	C2AA	Cl	1.744(8)
Ru1	C25	2.154(3)	C2AA	Cl1	1.721(9)
Ru1	C28	2.176(3)	C2AA	Cl2	1.681(9)
Ru1	C27	2.240(3)	C23	C28	1.406(4)
Ru1	C26	2.269(3)	C23	C24	1.422(4)
Ru1	C24	2.170(3)	N6	C5	1.458(3)
Cl33	C2AA	1.714(9)	N6	C2	1.360(3)
Cl34	C2AA	1.786(8)	N6	C7	1.378(4)
Cl32	C2AA	1.730(7)	C29	C26	1.518(4)
F13	C12	1.338(4)	N9	C10	1.473(3)
F19	C18	1.328(4)	N9	C2	1.365(3)
F15	C14	1.340(4)	N9	C8	1.385(4)
F21	C20	1.343(4)	C20	C18	1.380(4)
F17	C16	1.343(3)	C18	C16	1.371(5)
C22	C23	1.509(4)	C25	C26	1.436(4)
C30	C29	1.517(5)	C25	C24	1.403(4)
C14	C12	1.379(4)	C8	C7	1.336(4)
C14	C16	1.366(5)	C28	C27	1.417(4)
C31	C29	1.515(5)	C27	C26	1.388(4)

Table S5 Bond Angles for PhF-Ru (**1**).

Atom	Atom	Atom	Angle/˚	Atom	Atom	Atom	Angle/˚
Cl4	Ru1	Cl3	84.65(2)	Cl2	C2AA	Cl32	92.6(5)
C23	Ru1	Cl4	120.36(8)	Cl2	C2AA	Cl	108.1(5)
C23	Ru1	Cl3	154.98(8)	Cl2	C2AA	Cl1	111.7(4)
C23	Ru1	C27	67.23(11)	C22	C23	Ru1	131.0(2)
C23	Ru1	C26	80.12(11)	C28	C23	Ru1	70.26(17)
C2	Ru1	Cl4	90.05(7)	C28	C23	C22	120.9(3)
C2	Ru1	Cl3	89.81(8)	C28	C23	C24	117.9(3)
C2	Ru1	C23	90.61(11)	C24	C23	Ru1	69.81(16)
C2	Ru1	C25	118.46(10)	C24	C23	C22	121.3(3)
C2	Ru1	C28	117.09(11)	F13	C12	C14	117.8(3)
C2	Ru1	C27	154.49(11)	F13	C12	C11	120.1(2)
C2	Ru1	C26	156.23(10)	C11	C12	C14	122.1(3)
C2	Ru1	C24	91.29(11)	C2	N6	C5	127.3(2)
C25	Ru1	Cl4	150.93(8)	C2	N6	C7	111.5(2)
C25	Ru1	Cl3	89.58(8)	C7	N6	C5	121.3(2)
C25	Ru1	C23	68.37(11)	C30	C29	C26	110.6(3)
C25	Ru1	C28	79.99(11)	C31	C29	C30	111.3(3)
C25	Ru1	C27	66.35(10)	C31	C29	C26	113.5(3)
C25	Ru1	C26	37.77(10)	C2	N9	C10	124.6(2)
C25	Ru1	C24	37.87(11)	C2	N9	C8	111.6(2)
C28	Ru1	Cl4	92.45(8)	C8	N9	C10	123.7(2)
C28	Ru1	Cl3	152.99(9)	F21	C20	C11	119.1(2)
C28	Ru1	C23	37.45(11)	F21	C20	C18	118.1(3)
C28	Ru1	C27	37.41(12)	C11	C20	C18	122.8(3)
C28	Ru1	C26	66.91(11)	N9	C10	C11	112.0(2)
C27	Ru1	Cl4	90.63(7)	F19	C18	C20	121.0(3)
C27	Ru1	Cl3	115.64(8)	F19	C18	C16	120.4(3)
C27	Ru1	C26	35.86(10)	C16	C18	C20	118.6(3)
C26	Ru1	Cl4	113.55(7)	N6	C2	Ru1	128.08(19)
C26	Ru1	Cl3	89.64(8)	N6	C2	N9	103.3(2)
C24	Ru1	Cl4	158.27(8)	N9	C2	Ru1	128.28(19)
C24	Ru1	Cl3	117.04(8)	F17	C16	C14	119.7(3)
C24	Ru1	C23	37.94(11)	F17	C16	C18	119.8(3)
C24	Ru1	C28	67.73(11)	C14	C16	C18	120.5(3)
C24	Ru1	C27	79.03(11)	C26	C25	Ru1	75.46(15)
C24	Ru1	C26	67.97(11)	C24	C25	Ru1	71.68(16)
F15	C14	C12	120.4(3)	C24	C25	C26	122.0(2)
F15	C14	C16	120.1(3)	C7	C8	N9	106.3(2)
C16	C14	C12	119.6(3)	C23	C28	Ru1	72.30(17)
C12	C11	C20	116.5(2)	C23	C28	C27	121.2(3)
C12	C11	C10	121.9(3)	C27	C28	Ru1	73.76(16)
C20	C11	C10	121.5(3)	C28	C27	Ru1	68.83(16)
Cl33	C2AA	Cl34	109.2(4)	C26	C27	Ru1	73.21(16)

Cl33	C2AA	Cl32	112.9(5)	C26	C27	C28	121.8(3)
Cl33	C2AA	Cl	96.7(4)	C29	C26	Ru1	129.3(2)
Cl33	C2AA	Cl1	17.3(3)	C25	C26	Ru1	66.77(15)
Cl32	C2AA	Cl34	110.7(5)	C25	C26	C29	119.2(2)
Cl32	C2AA	Cl	17.2(6)	C27	C26	Ru1	70.93(16)
Cl	C2AA	Cl34	123.9(5)	C27	C26	C29	123.9(3)
Cl1	C2AA	Cl34	91.8(4)	C27	C26	C25	116.8(3)
Cl1	C2AA	Cl32	121.2(5)	C8	C7	N6	107.4(3)
Cl1	C2AA	Cl	107.1(5)	C23	C24	Ru1	72.25(16)
Cl2	C2AA	Cl33	128.9(4)	C25	C24	Ru1	70.44(16)
Cl2	C2AA	Cl34	21.5(3)	C25	C24	C23	120.1(3)

Table S6 Hydrogen Atom Coordinates (Å×10^4) and Isotropic Displacement Parameters (Å^2×10^3) for PhF-Ru (**1**).

Atom	***x***	***y***	***z***	**U(eq)**
H22A	4352	3607	6717	73
H22B	3761	2486	6946	73
H22C	3551	3856	7244	73
H30A	745	3323	3013	106
H30B	751	3218	4013	106
H30C	1314	2319	3483	106
H31A	2551	3299	2701	100
H31B	2728	4740	2826	100
H31C	1933	4294	2292	100
H2AA	6818	11245	5159	71
H2AB	6806	11271	5093	71
H29	1540	4935	3630	44
H10A	1506	6201	6326	38
H10B	1550	7676	6318	38
H5A	4698	5638	6115	61
H5B	5043	5923	7045	61
H5C	5008	6996	6357	61
H25	1380	4203	5224	33
H8	2656	7814	8050	44
H28	4241	3477	5164	41
H27	3455	3615	3887	37
H7	4165	7459	7974	47
H24	2127	3829	6496	38

Table S7 Atomic Occupancy for PhF-Ru (**1**).

Atom	***Occupancy***	**Atom**	***Occupancy***	**Atom**	***Occupancy***
Cl33	0.50	Cl34	0.50	Cl32	0.50
H2AA	0.50	H2AB	0.50	Cl	0.50
Cl1	0.50	Cl2	0.50		

Experimental

Single crystals of $C_{22}H_{22}Cl_5F_5N_2Ru$ (PhF-Ru (**1**)) were mounted on a MicroMount® polymer tip (MiteGen) in a random orientation. Data collection was performed on a SuperNova dual source equipped with a CCD Atlas detector diffractometer (Agilent Technologies). The crystal was kept at 293(2) K during data collection. Using Olex2 [1], the structure was solved with the Superflip [2] structure solution program using Charge Flipping and refined with the ShelXL [3] refinement package using Least Squares minimisation.

1. Dolomanov, O.V., Bourhis, L.J., Gildea, R.J, Howard, J.A.K. & Puschmann, H. (2009), J. Appl. Cryst. 42, 339-341.
2. Palatinus, L. & Chapuis, G. (2007). J. Appl. Cryst., 40, 786-790; Palatinus, L. & van der Lee, A. (2008). J. Appl. Cryst. 41, 975-984; Palatinus, L., Prathapa, S. J. & van Smaalen, S. (2012). J. Appl. Cryst. 45, 575-580.
3. Sheldrick, G.M. (2008). Acta Cryst. A64, 112-122.

Crystal structure determination of PhF-Ru (**1**).

Crystal Data for $C_{22}H_{22}Cl_5F_5N_2Ru$ (M=687.74 g/mol): monoclinic, space group $P2_1/c$ (no. 14), a = 15.9690(4) Å, b = 10.6225(4) Å, c = 15.6395(5) Å, β = 91.922(3)°, V = 2651.44(15) Å^3, Z = 4, T = 293(2) K, μ(MoKα) = 1.146 mm^{-1}, *Dcalc* = 1.723 g/cm^3, 29917 reflections measured (5.72° ≤ 2Θ ≤ 58.92°), 6622 unique (R_{int} = 0.0518, R_{sigma} = 0.0391) which were used in all calculations. The final R_1 was 0.0351 (>2sigma(I)) and wR_2 was 0.0997 (all data).

Crystallographic data and structure refinement for compound Pyr-Ru (**3**).

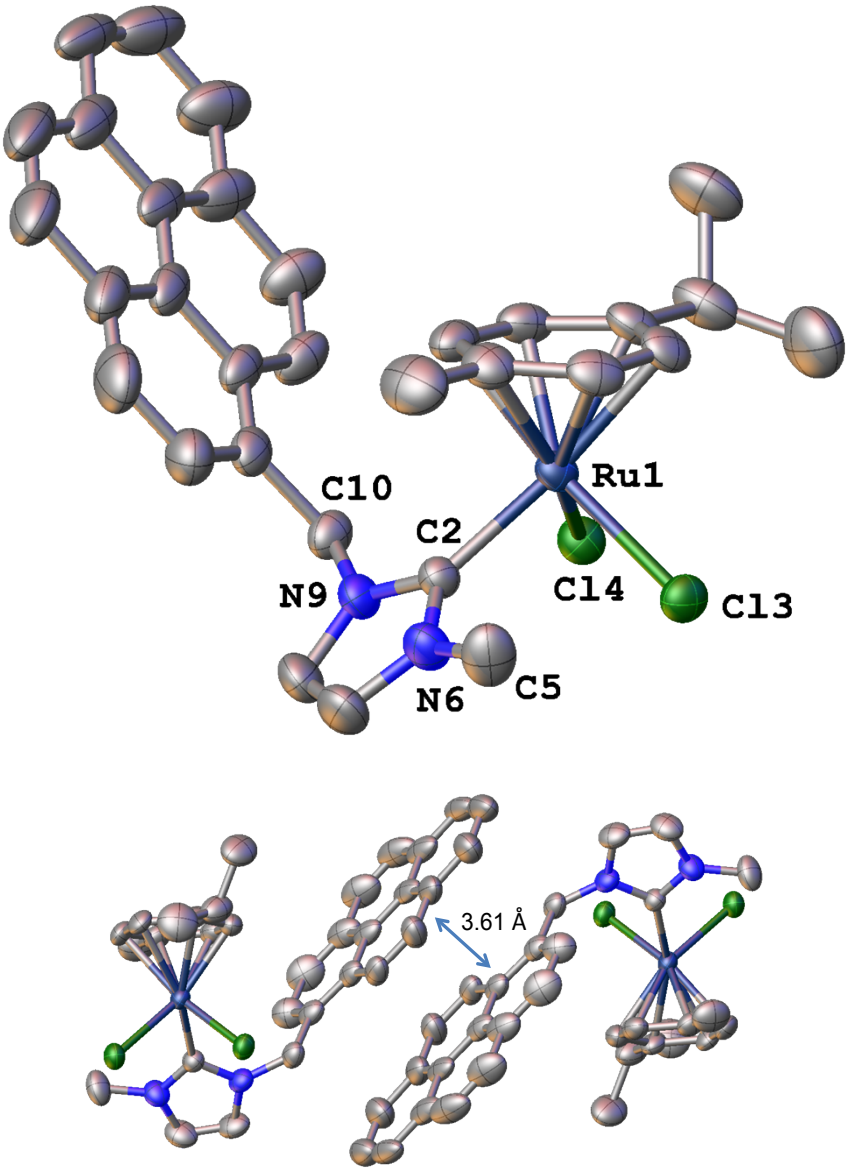

Molecular diagram (top) and crystal packing (bottom) of compound Pyr-Ru (**3**). Ellipsoids are at 50% probability level. Hydrogen atoms and crystallization solvents (chloroform and n-hexane) omitted for clarity. Selected bond lengths [Å] and angles [º]: Ru(1) - C(2) 2.081(3), Ru(1) - Cl(3) 2.4282(10), Ru(1) - Cl(4) 2.4312(9), Ru(1) - Ph_{cent} 1.684, C(2) - N(6) 1.354(5), C(2) - N(9) 1.360(5), Cl(3) - Ru(1) - Cl(4) 84.16(3), C(2) - Ru(1) - Cl(3) 91.02(10), C(2) - Ru(1) - Cl(4) 88.03(10), N(6) - C(2) - N(9) 104.1(3).

Table S8 Crystal data and structure refinement for Pyr-Ru (**3**).

Identification code	str1743
Empirical formula	$C_{36}H_{39}Cl_8N_2Ru$
Formula weight	884.36
Temperature/K	293(2)
Crystal system	triclinic
Space group	P-1
a/Å	11.3681(4)
b/Å	14.3155(7)
c/Å	14.8357(7)
α/°	62.367(5)
β/°	84.064(4)
γ/°	77.725(4)
Volume/Å^3	2090.06(17)
Z	2
ρ_{calc}g/cm^3	1.405
μ/mm^{-1}	0.913
F(000)	898.0
Crystal size/mm^3	0.13 × 0.1 × 0.09
Radiation	MoKα (λ = 0.71073)
2Θ range for data collection/°	5.82 to 59.06
Index ranges	-15 ≤ h ≤ 15, -19 ≤ k ≤ 19, -20 ≤ l ≤ 20
Reflections collected	45813
Independent reflections	10614 [R_{int} = 0.0570, R_{sigma} = 0.0449]
Data/restraints/parameters	10614/81/491
Goodness-of-fit on F^2	1.069
Final R indexes [I>=2σ (I)]	R_1 = 0.0613, wR_2 = 0.1725
Final R indexes [all data]	R_1 = 0.0766, wR_2 = 0.1917
Largest diff. peak/hole / e Å^{-3}	1.80/-0.98

Table S9 Fractional Atomic Coordinates (×10^4) and Equivalent Isotropic Displacement Parameters (Å^2×10^3) for Pyr-Ru (**3**). U_{eq} is defined as 1/3 of of the trace of the orthogonalised U_{IJ} tensor.

Atom	*x*	*y*	*z*	U(eq)
Ru1	2915.5(2)	4285.2(2)	1754.3(2)	32.45(11)
Cl3	2794.7(9)	6066.5(7)	331.2(7)	41.4(2)
Cl4	1184.7(8)	5130.5(8)	2396.0(7)	39.7(2)
C22	2407(5)	-1977(5)	7367(6)	84(2)
C21	2247(4)	-1504(4)	6306(5)	73.4(18)
C26	2429(6)	-1616(4)	4708(6)	83(2)
C25	2582(5)	-2073(4)	5721(7)	91(2)
C5	2573(5)	4588(4)	-723(3)	59.0(12)
C16	1072(4)	1233(3)	4174(4)	47.6(10)
N9	751(3)	3438(3)	1478(3)	41.2(7)
C36	4124(7)	5815(6)	3093(6)	88(2)
C14	1919(5)	-482(4)	4162(5)	68.1(15)
C27	4496(5)	2309(5)	1227(5)	74.0(16)
N6	1687(3)	4133(3)	63(3)	45.7(8)
C33	3624(4)	2614(3)	2744(3)	48.3(10)
C15	1568(4)	116(3)	4705(4)	53.9(11)
C8	115(4)	3399(4)	755(4)	55.2(11)
C13	1780(6)	31(4)	3113(6)	75.5(16)
C35	4541(6)	4051(6)	4623(5)	79.1(17)
C20	1722(4)	-393(3)	5787(4)	59.1(14)
C24	1578(6)	-332(5)	7398(5)	84.4(19)
C30	4726(3)	4397(4)	2106(3)	44.6(9)
C23	2072(6)	-1394(6)	7902(6)	93(2)
C18	874(5)	1303(4)	5800(4)	66.2(14)
C7	694(5)	3835(4)	-128(4)	58.7(12)
C32	3470(4)	3199(3)	3296(3)	46.5(9)
C17	732(4)	1789(3)	4785(4)	54.7(11)
C2	1719(3)	3914(3)	1052(3)	34.5(7)
C11	960(4)	1732(3)	3120(4)	46.0(9)
C28	4319(4)	2929(4)	1832(3)	46.7(9)
C12	1307(5)	1138(4)	2587(5)	62.8(13)
C31	4056(3)	4093(4)	3010(3)	45.3(9)
C19	1389(5)	193(5)	6342(4)	69.3(16)
C29	4829(3)	3850(4)	1512(3)	46.3(9)
C10	464(4)	2929(3)	2560(3)	43.3(8)
C34	3853(5)	4696(5)	3641(4)	61.8(13)
Cl44	8225(6)	6461(4)	4006(5)	118.1(19)
Cl46	8685(4)	4173(3)	5148(3)	97.4(11)
Cl42	7817(4)	5091(6)	3150(4)	125.7(18)
C41	8701(6)	5456(8)	3812(6)	102(3)
Cl43	7736(7)	6572(6)	2692(5)	162(2)
Cl45	8671(5)	6095(6)	4571(5)	118(2)
Cl47	8260(5)	4422(5)	4165(7)	156(3)

Cl39	2417(4)	8660(3)	663(4)	200.1(18)
C37	1257(9)	7906(6)	1192(7)	112(3)
Cl40	1056(4)	7838(3)	2393(3)	191.8(16)
Cl38	70(5)	8454(4)	437(6)	278(4)
C50	4439(15)	908(12)	5615(13)	57(4)
C49	4737(14)	204(12)	6206(11)	52(4)
C51	4903(12)	159(13)	5270(11)	94(5)
C52	5120(50)	-340(40)	620(30)	290(20)
C53	5670(40)	-1650(40)	1150(40)	252(18)
C54	6820(40)	-1290(30)	250(30)	228(17)
C48	4382(12)	931(10)	6631(11)	94(4)

Table S10 Anisotropic Displacement Parameters ($Å^2 \times 10^3$) for Pyr-Ru (**3**). The Anisotropic displacement factor exponent takes the form: $-2\pi^2[h^2a^{*2}U_{11}+2hka^*b^*U_{12}+\ldots]$.

Atom	U_{11}	U_{22}	U_{33}	U_{23}	U_{13}	U_{12}
Ru1	26.33(16)	38.89(18)	31.27(17)	-14.46(12)	1.85(10)	-8.92(11)
Cl3	40.3(5)	41.9(5)	37.0(4)	-13.1(4)	4.8(3)	-11.8(4)
Cl4	35.0(4)	45.8(5)	39.6(4)	-21.0(4)	5.5(3)	-9.1(4)
C22	43(3)	53(3)	96(5)	22(3)	-21(3)	-17(2)
C21	36(2)	44(2)	105(4)	0(3)	-7(2)	-15.6(19)
C26	67(4)	39(2)	130(6)	-27(3)	-14(4)	-7(2)
C25	58(3)	37(2)	143(7)	-7(3)	-27(4)	-8(2)
C5	78(3)	66(3)	40(2)	-27(2)	12(2)	-28(3)
C16	33.1(19)	33.2(18)	62(3)	-7.5(17)	2.5(17)	-12.0(15)
N9	33.5(16)	40.6(16)	48.3(18)	-16.0(14)	-4.0(13)	-12.8(13)
C36	105(5)	89(4)	96(5)	-62(4)	-12(4)	-21(4)
C14	50(3)	39(2)	103(4)	-18(3)	-10(3)	-13(2)
C27	68(3)	73(3)	89(4)	-52(3)	-10(3)	11(3)
N6	52(2)	49.9(19)	39.0(17)	-19.8(15)	-5.5(14)	-15.3(16)
C33	35(2)	39.8(19)	54(2)	-7.1(18)	-8.8(17)	-5.3(16)
C15	32(2)	34.0(19)	82(3)	-12(2)	-1.1(19)	-13.4(15)
C8	44(2)	54(2)	71(3)	-26(2)	-15(2)	-16.1(19)
C13	77(4)	52(3)	112(5)	-49(3)	-5(3)	-14(3)
C35	74(4)	116(5)	65(3)	-55(4)	-15(3)	-13(3)
C20	29(2)	40(2)	79(3)	2(2)	-6(2)	-16.4(16)
C24	68(4)	84(4)	61(3)	3(3)	-4(3)	-18(3)
C30	26.0(17)	57(2)	51(2)	-21.9(19)	-1.0(15)	-13.8(16)
C23	58(3)	87(5)	75(4)	17(4)	-14(3)	-18(3)
C18	64(3)	57(3)	53(3)	-8(2)	8(2)	-6(2)
C7	68(3)	61(3)	55(3)	-26(2)	-19(2)	-17(2)
C32	35.0(19)	54(2)	36.5(19)	-8.9(17)	-4.4(15)	-7.3(17)
C17	46(2)	38(2)	58(3)	-5.7(19)	9.0(19)	-6.4(17)
C2	31.7(17)	35.3(17)	35.8(17)	-14.2(14)	-1.3(13)	-8.8(13)
C11	31.8(19)	38.0(19)	63(3)	-16.3(18)	-0.2(17)	-12.9(15)
C28	32.9(19)	51(2)	56(2)	-26.2(19)	-3.4(17)	1.0(16)
C12	64(3)	50(2)	78(3)	-29(2)	-11(3)	-12(2)
C31	30.0(18)	64(3)	44(2)	-24.1(19)	-6.3(15)	-10.3(17)
C19	47(3)	63(3)	61(3)	5(2)	5(2)	-16(2)
C29	25.2(17)	63(2)	46(2)	-22.5(19)	4.0(15)	-5.0(16)
C10	35.6(19)	36.5(18)	50(2)	-12.1(16)	4.2(16)	-11.0(15)
C34	47(3)	89(4)	61(3)	-46(3)	-8(2)	-5(2)
Cl44	118(5)	84(3)	144(5)	-52(3)	47(4)	-25(3)
Cl46	108(3)	91(2)	82(2)	-39.2(19)	12(2)	-3(2)
Cl42	95(3)	210(6)	96(3)	-79(3)	-3(2)	-51(3)
C41	63(4)	171(8)	118(6)	-108(6)	20(4)	-20(4)
Cl43	176(6)	184(6)	134(4)	-88(4)	-12(4)	-5(5)
Cl45	102(4)	168(6)	138(5)	-116(5)	31(3)	-39(4)
Cl47	84(3)	116(4)	308(10)	-128(5)	43(4)	-43(3)
Cl39	221(4)	139(3)	261(5)	-94(3)	71(3)	-102(3)

C37	160(8)	75(4)	116(6)	-59(4)	35(6)	-27(5)
Cl40	235(4)	218(4)	206(3)	-173(3)	62(3)	-54(3)
Cl38	242(5)	179(3)	493(9)	-231(5)	-199(6)	84(3)
C50	37(7)	45(7)	63(8)	6(6)	-13(6)	-23(6)
C49	28(6)	38(6)	66(8)	1(6)	-8(6)	-12(5)
C51	47(5)	117(8)	115(9)	-37(6)	14(6)	-56(6)
C52	290(20)	290(20)	290(20)	-134(14)	-3(10)	-63(11)
C53	250(20)	250(20)	250(20)	-114(12)	0(10)	-40(10)
C54	300(40)	220(30)	260(40)	-160(30)	-40(30)	-100(30)
C48	69(6)	77(6)	101(7)	-6(5)	-6(6)	-27(5)

Table S11 Bond Lengths for Pyr-Ru (**3**).

Atom	Atom	Length/Å	Atom	Atom	Length/Å
Ru1	Cl3	2.4282(10)	C13	C12	1.409(7)
Ru1	Cl4	2.4312(9)	C35	C34	1.507(7)
Ru1	C33	2.167(4)	C20	C19	1.402(9)
Ru1	C30	2.230(4)	C24	C23	1.362(10)
Ru1	C32	2.151(4)	C24	C19	1.405(8)
Ru1	C2	2.081(3)	C30	C31	1.397(6)
Ru1	C28	2.200(4)	C30	C29	1.409(6)
Ru1	C31	2.258(4)	C18	C17	1.345(7)
Ru1	C29	2.172(4)	C18	C19	1.425(7)
C22	C21	1.410(10)	C32	C31	1.437(6)
C22	C23	1.374(11)	C11	C12	1.386(7)
C21	C25	1.420(11)	C11	C10	1.520(5)
C21	C20	1.426(6)	C28	C29	1.410(6)
C26	C25	1.346(11)	C31	C34	1.515(7)
C26	C14	1.450(7)	Cl44	C41	1.570(10)
C5	N6	1.459(6)	Cl46	C41	1.983(10)
C16	C15	1.426(6)	Cl42	C41	1.775(8)
C16	C17	1.439(7)	C41	Cl43	1.919(11)
C16	C11	1.393(7)	C41	Cl45	1.744(8)
N9	C8	1.383(5)	C41	Cl47	1.503(10)
N9	C2	1.360(5)	Cl39	C37	1.767(10)
N9	C10	1.456(5)	C37	Cl40	1.732(9)
C36	C34	1.507(9)	C37	Cl38	1.656(11)
C14	C15	1.403(8)	C50	C51	1.379(10)
C14	C13	1.389(9)	C50	C48	1.52(2)
C27	C28	1.503(7)	C49	C51	1.411(9)
N6	C7	1.386(6)	C49	C48	1.423(9)
N6	C2	1.354(5)	C51	C51[1]	1.08(2)
C33	C32	1.395(7)	C52	C52[2]	1.66(8)
C33	C28	1.422(6)	C52	C53	1.67(5)
C15	C20	1.435(8)	C53	C54	1.75(5)
C8	C7	1.333(7)			

[1]1-X,-Y,1-Z; [2]1-X,-Y,-Z

Table S12 Bond Angles for Pyr-Ru (**3**).

Atom	Atom	Atom	Angle/°	Atom	Atom	Atom	Angle/°
Cl3	Ru1	Cl4	84.16(3)	C31	C30	Ru1	73.0(2)
C33	Ru1	Cl3	159.33(13)	C31	C30	C29	121.8(4)
C33	Ru1	Cl4	116.19(13)	C29	C30	Ru1	69.1(2)
C33	Ru1	C30	79.19(16)	C24	C23	C22	119.5(7)
C33	Ru1	C28	38.00(17)	C17	C18	C19	121.6(6)
C33	Ru1	C31	68.06(17)	C8	C7	N6	106.9(4)
C33	Ru1	C29	67.84(17)	C33	C32	Ru1	71.8(2)
C30	Ru1	Cl3	88.53(11)	C33	C32	C31	122.1(4)
C30	Ru1	Cl4	116.68(12)	C31	C32	Ru1	75.1(2)
C30	Ru1	C31	36.27(15)	C18	C17	C16	123.0(4)
C32	Ru1	Cl3	148.13(13)	N9	C2	Ru1	127.5(3)
C32	Ru1	Cl4	89.33(12)	N6	C2	Ru1	128.3(3)
C32	Ru1	C33	37.68(18)	N6	C2	N9	104.1(3)
C32	Ru1	C30	66.71(16)	C16	C11	C10	119.7(4)
C32	Ru1	C28	68.38(17)	C12	C11	C16	119.9(4)
C32	Ru1	C31	37.94(16)	C12	C11	C10	120.4(4)
C32	Ru1	C29	80.08(16)	C27	C28	Ru1	131.0(3)
C2	Ru1	Cl3	91.02(10)	C33	C28	Ru1	69.8(2)
C2	Ru1	Cl4	88.03(10)	C33	C28	C27	121.3(5)
C2	Ru1	C33	93.22(15)	C29	C28	Ru1	70.1(2)
C2	Ru1	C30	155.08(16)	C29	C28	C27	121.2(5)
C2	Ru1	C32	119.97(15)	C29	C28	C33	117.5(4)
C2	Ru1	C28	91.96(15)	C11	C12	C13	119.9(5)
C2	Ru1	C31	157.86(16)	C30	C31	Ru1	70.8(2)
C2	Ru1	C29	117.89(16)	C30	C31	C32	116.5(4)
C28	Ru1	Cl3	121.67(13)	C30	C31	C34	123.8(4)
C28	Ru1	Cl4	154.16(13)	C32	C31	Ru1	67.0(2)
C28	Ru1	C30	67.41(16)	C32	C31	C34	119.6(4)
C28	Ru1	C31	80.50(16)	C34	C31	Ru1	129.3(3)
C31	Ru1	Cl3	110.69(12)	C20	C19	C24	119.0(6)
C31	Ru1	Cl4	89.90(11)	C20	C19	C18	118.0(5)
C29	Ru1	Cl3	92.35(12)	C24	C19	C18	123.0(7)
C29	Ru1	Cl4	153.95(12)	C30	C29	Ru1	73.6(2)
C29	Ru1	C30	37.30(16)	C30	C29	C28	121.4(4)
C29	Ru1	C28	37.62(17)	C28	C29	Ru1	72.3(2)
C29	Ru1	C31	67.17(16)	N9	C10	C11	115.1(4)
C23	C22	C21	121.6(5)	C36	C34	C31	114.5(5)
C22	C21	C25	123.6(6)	C35	C34	C36	110.8(5)
C22	C21	C20	118.5(7)	C35	C34	C31	110.5(4)
C25	C21	C20	117.9(6)	Cl44	C41	Cl46	106.6(4)
C25	C26	C14	119.7(7)	Cl44	C41	Cl42	121.1(6)
C26	C25	C21	123.3(5)	Cl44	C41	Cl43	69.4(5)
C15	C16	C17	116.3(4)	Cl44	C41	Cl45	30.8(3)
C11	C16	C15	120.2(5)	Cl42	C41	Cl46	96.9(5)

C11	C16	C17	123.5(4)	Cl42	C41	Cl43	61.3(4)
C8	N9	C10	122.8(4)	Cl43	C41	Cl46	145.2(5)
C2	N9	C8	110.9(4)	Cl45	C41	Cl46	82.8(4)
C2	N9	C10	126.0(3)	Cl45	C41	Cl42	145.3(5)
C15	C14	C26	119.3(6)	Cl45	C41	Cl43	100.2(5)
C13	C14	C26	121.7(6)	Cl47	C41	Cl44	132.1(6)
C13	C14	C15	119.0(4)	Cl47	C41	Cl46	46.4(5)
C7	N6	C5	122.3(4)	Cl47	C41	Cl42	51.0(4)
C2	N6	C5	126.6(3)	Cl47	C41	Cl43	109.3(6)
C2	N6	C7	111.0(4)	Cl47	C41	Cl45	123.5(7)
C32	C33	Ru1	70.5(2)	Cl40	C37	Cl39	103.2(5)
C32	C33	C28	120.5(4)	Cl38	C37	Cl39	110.7(6)
C28	C33	Ru1	72.2(2)	Cl38	C37	Cl40	116.9(6)
C16	C15	C20	120.3(5)	C51	C50	C48	135.5(14)
C14	C15	C16	119.7(5)	C51	C49	C48	142.4(15)
C14	C15	C20	120.0(4)	C50	C51	C49	41.9(10)
C7	C8	N9	107.0(4)	C51[1]	C51	C50	157(3)
C14	C13	C12	121.3(6)	C51[1]	C51	C49	161(3)
C21	C20	C15	119.8(6)	C52[2]	C52	C53	120(5)
C19	C20	C21	119.3(5)	C52	C53	C54	84(3)
C19	C20	C15	120.8(4)	C49	C48	C50	39.5(9)
C23	C24	C19	122.1(8)				

[1]1-X,-Y,1-Z; [2]1-X,-Y,-Z

Table S13 Hydrogen Atom Coordinates (Å×10^4) and Isotropic Displacement Parameters (Å^2×10^3) for Pyr-Ru (**3**).

Atom	*x*	*y*	*z*	U(eq)
H22	2746	-2702	7714	101
H26	2649	-2025	4359	99
H25	2926	-2797	6055	109
H5A	2940	4080	-968	88
H5B	3180	4751	-442	88
H5C	2182	5234	-1275	88
H36A	3892	6169	3515	132
H36B	3681	6211	2468	132
H36C	4970	5777	2948	132
H27A	3794	2009	1292	111
H27B	5185	1742	1478	111
H27C	4622	2781	524	111
H33	3270	2013	2975	58
H8	-584	3120	864	66
H13	2002	-363	2751	91
H35A	5381	4076	4491	119
H35B	4432	3320	4920	119
H35C	4248	4346	5086	119
H24	1360	59	7764	101
H30	5113	4977	1892	54
H23	2182	-1721	8602	111
H18	630	1701	6157	79
H7	473	3922	-753	70
H32	2972	3004	3867	56
H17	400	2516	4463	66
H12	1229	1469	1883	75
H29	5242	4102	896	56
H10A	-405	3043	2639	52
H10B	772	3284	2881	52
H34	2996	4767	3821	74
H41	9520	5470	3532	123
H41A	9526	5358	3561	123
H37	1557	7180	1266	135
H50A	3603	1122	5409	68
H50B	4810	1518	5168	68
H49A	5514	-173	6523	63
H49B	4202	-304	6561	63
H51C	5721	5	5502	112
H51D	4550	-427	5793	112
H51B	4130	599	4985	112
H51A	5450	663	4979	112
H52A	4362	-233	957	343
H52B	5668	-3	783	343
H53A	5169	-2078	1070	302

H53B	5925	-1956	1853	302
H54A	6476	-925	-420	342
H54B	7374	-1929	319	342
H54C	7228	-833	354	342
H48D	4338	1655	6518	140
H48E	5091	485	7016	140
H48F	3682	670	7001	140
H48A	4217	1652	6093	140
H48B	5019	863	7048	140
H48C	3671	771	7039	140

Table S14 Atomic Occupancy for Pyr-Ru (**3**).

Atom	*Occupancy*	Atom	*Occupancy*	Atom	*Occupancy*
Cl44	0.50	Cl46	0.50	Cl42	0.50
H41	0.50	H41A	0.50	Cl43	0.50
Cl45	0.50	Cl47	0.50	C50	0.25
H50A	0.25	H50B	0.25	C49	0.25
H49A	0.25	H49B	0.25	C51	0.50
H51C	0.25	H51D	0.25	H51B	0.25
H51A	0.25	C52	0.50	H52A	0.50
H52B	0.50	C53	0.50	H53A	0.50
H53B	0.50	C54	0.50	H54A	0.50
H54B	0.50	H54C	0.50	C48	0.50
H48D	0.25	H48E	0.25	H48F	0.25
H48A	0.25	H48B	0.25	H48C	0.25

Experimental

Single crystals of $C_{36}H_{39}Cl_8N_2Ru$ (Pyr-Ru (**3**)) were mounted on a MicroMount® polymer tip (MiteGen) in a random orientation. Data collection was performed on a SuperNova dual source equipped with a CCD Atlas detector diffractometer (Agilent Technologies). The crystal was kept at 293(2) K during data collection. Using Olex2 [1], the structure was solved with the Superflip [2] structure solution program using Charge Flipping and refined with the ShelXL [3] refinement package using Least Squares minimisation.

1. Dolomanov, O.V., Bourhis, L.J., Gildea, R.J, Howard, J.A.K. & Puschmann, H. (2009), J. Appl. Cryst. 42, 339-341.
2. Palatinus, L. & Chapuis, G. (2007). J. Appl. Cryst., 40, 786-790; Palatinus, L. & van der Lee, A. (2008). J. Appl. Cryst. 41, 975-984; Palatinus, L., Prathapa, S. J. & van Smaalen, S. (2012). J. Appl. Cryst. 45, 575-580.
3. Sheldrick, G.M. (2008). Acta Cryst. A64, 112-122.

Crystal structure determination of Pyr-Ru (**3**)

Crystal Data for $C_{36}H_{39}Cl_8N_2Ru$ (M =884.36 g/mol): triclinic, space group P-1 (no. 2), a = 11.3681(4) Å, b = 14.3155(7) Å, c = 14.8357(7) Å, α = 62.367(5)°, β = 84.064(4)°, γ = 77.725(4)°, V = 2090.06(17) Å^3, Z = 2, T = 293(2) K, μ(MoKα) = 0.913 mm^{-1}, $Dcalc$ = 1.405 g/cm^3, 45813 reflections measured (5.82° ≤ 2Θ ≤ 59.06°), 10614 unique (R_{int} = 0.0570, R_{sigma} = 0.0449) which were used in all calculations. The final R_1 was 0.0613 (>2sigma(I)) and wR_2 was 0.1917 (all data).

5. UV/Vis spectroscopy

The UV/Vis spectra were recorded between 250 and 600 nm by a Cary 300 Bio UV−Vis Varian spectrophotometer. The samples were suspended in DMF and sonicated for 5 minutes before measurement. The molecular complexes were dissolved in DMF (10^{-6}M)

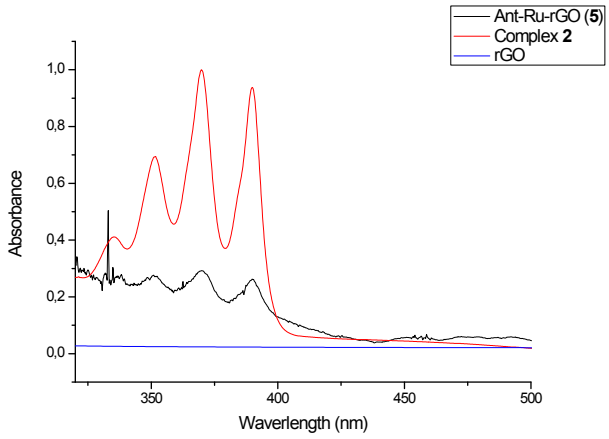

Figure S1 UV/Vis spectra of **rGO**, complex Ant-Ru (**2**) and Ant-Ru-rGO (**5**)

6. FTIR Spectroscopy

Infrared spectra (FTIR) were performed on a JASCO FT/IR-6200 spectrometer with a spectral window of 4000-500 cm^{-1}. The samples were prepared as KBr disks.

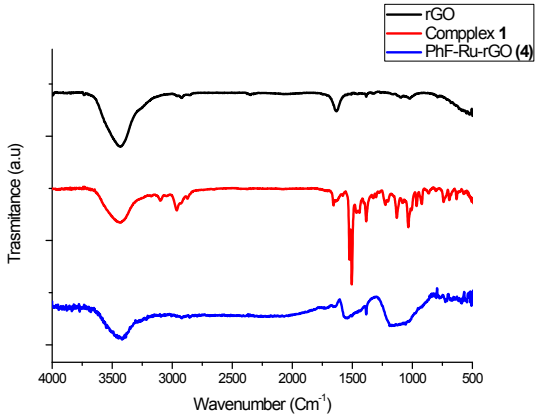

Figure S2 FTIR spectra of rGO, PhF-Ru (**1**) and PhF-Ru-rGO (**4**).

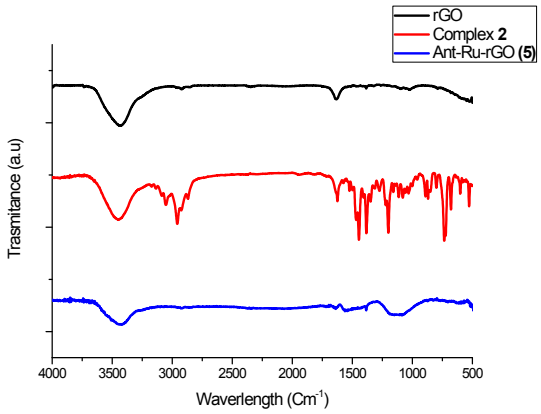

Figure S3. FTIR spectra of **rGO**, complex Ant-Ru (**2**) and Ant-Ru-rGO (**5**)

7. High Resolution Transmission Electron Microscopy (HRTEM) images

High-resolution images of transmission electron microscopy HRTEM and high-angle annular dark-field HAADF-STEM images of the samples were obtained using a Jem-2100 LaB6 (JEOL) transmission electron microscope coupled with an INCA Energy TEM 200 (Oxford) energy dispersive X-Ray spectrometer (EDX) operating at 200 kV. Samples were prepared by drying a droplet of a MeOH dispersion on a carbon-coated copper grid.

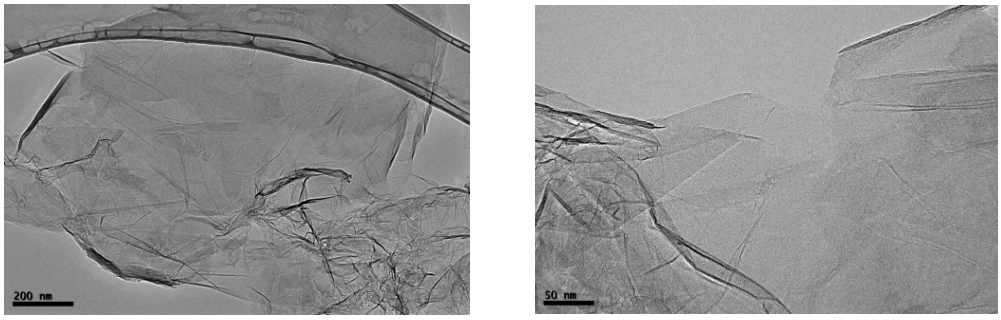

Figure S4. HRTEM images of PhF-Ru-rGO (**4**).

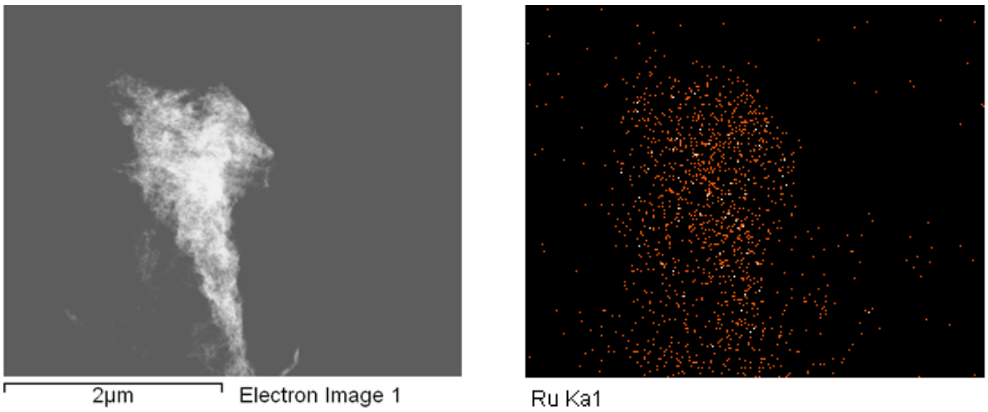

Figure S5. STEM image of PhF-Ru-rGO (**4**) (left) and EDS elemental mapping image showing the homogeneous distribution of ruthenium (right).

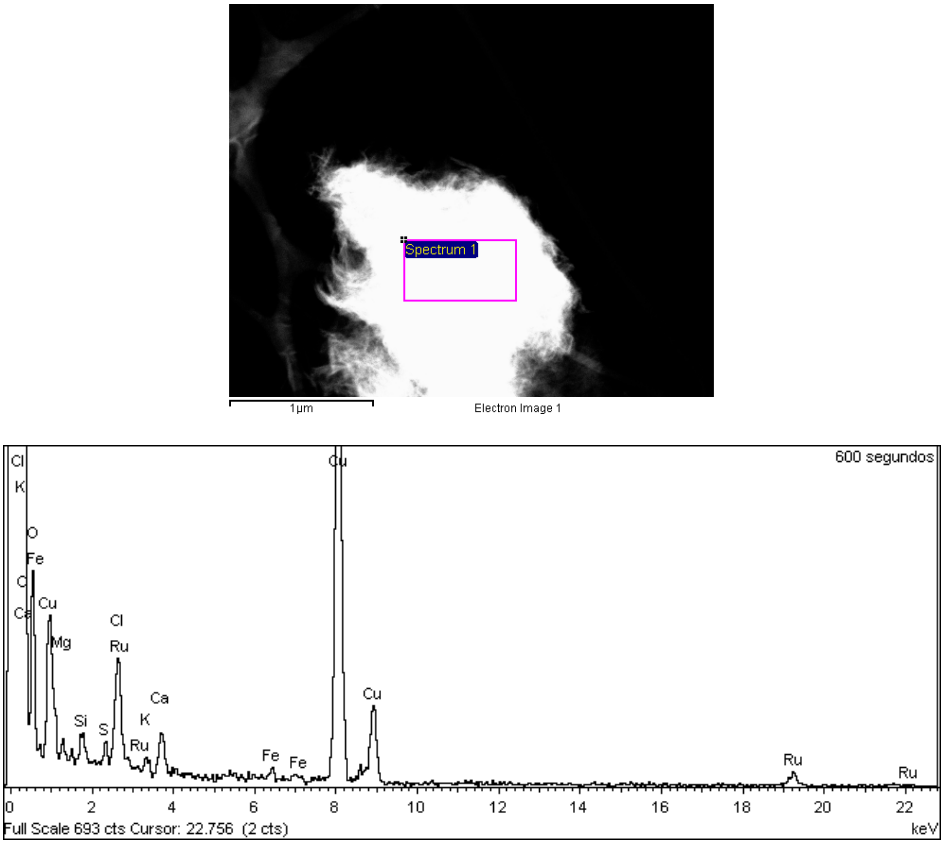

Figure S6. STEM image (top) and EDS spectrum (bottom) of PhF-Ru-rGO (**4**).

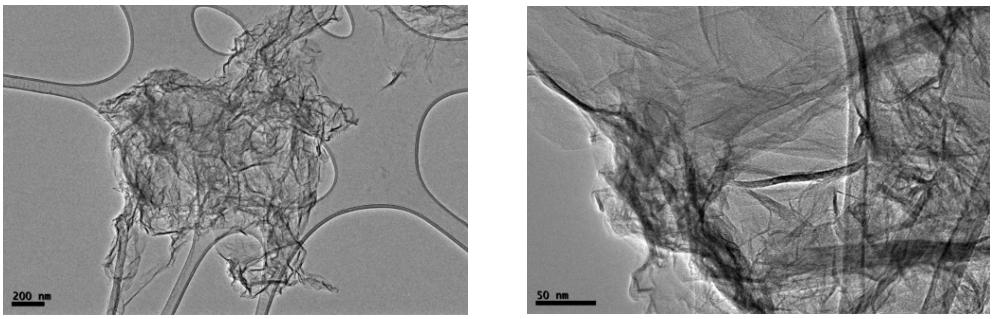

Figure S7. HRTEM images of Ant-Ru-rGO (**5**)

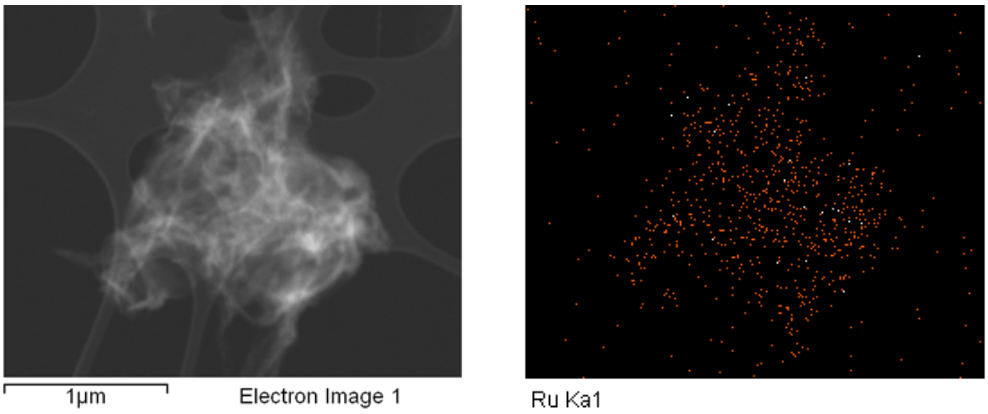

Figure S8. STEM image of Ant-Ru-rGO (**5**) (left) and EDS elemental mapping image showing the homogeneous distribution of ruthenium (right).

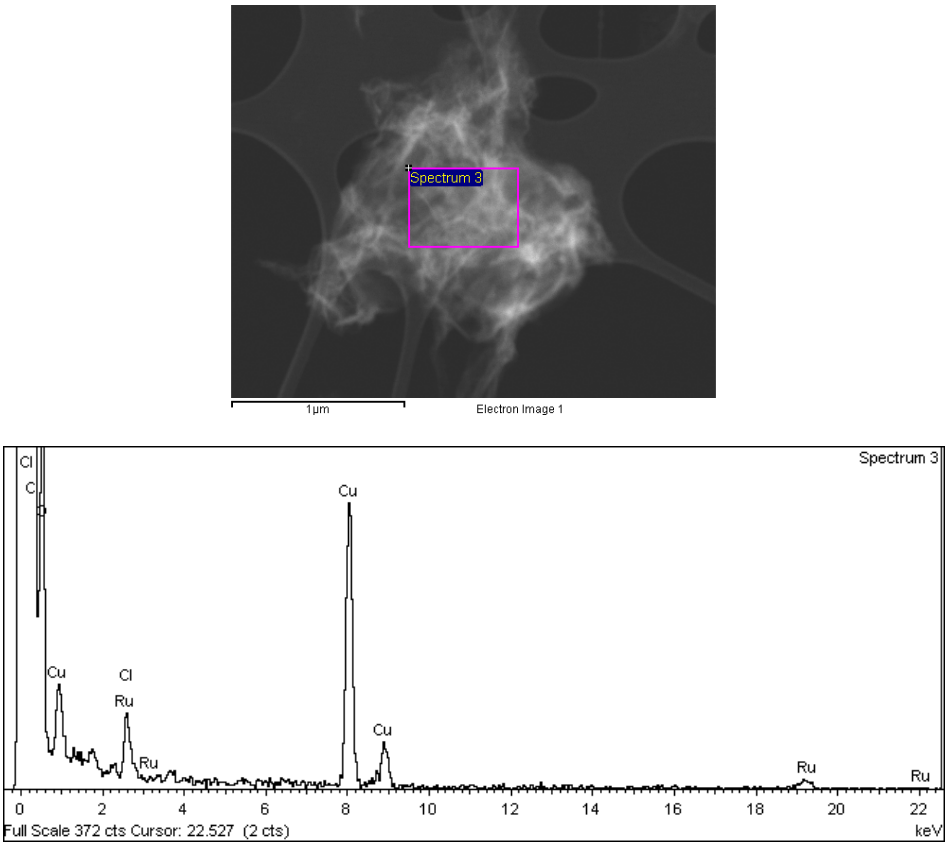

Figure S9. STEM image (top) and EDS spectrum (bottom) of Ant-Ru-rGO (**5**).

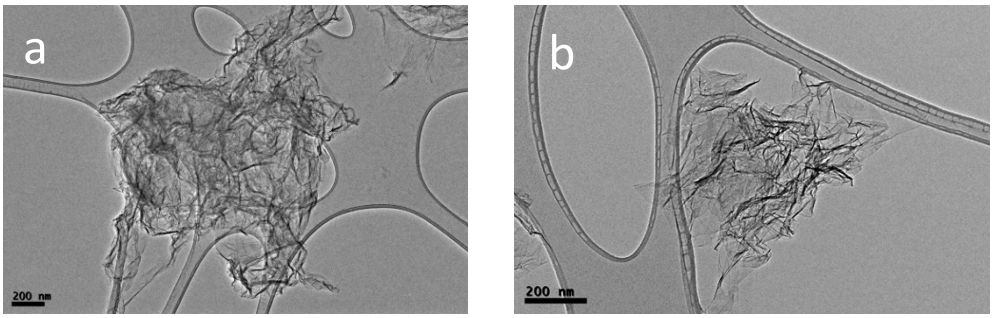

Figure S10. HRTEM images of Ant-Ru-rGO (**5**) before (left) and after (right) ten catalytic runs.

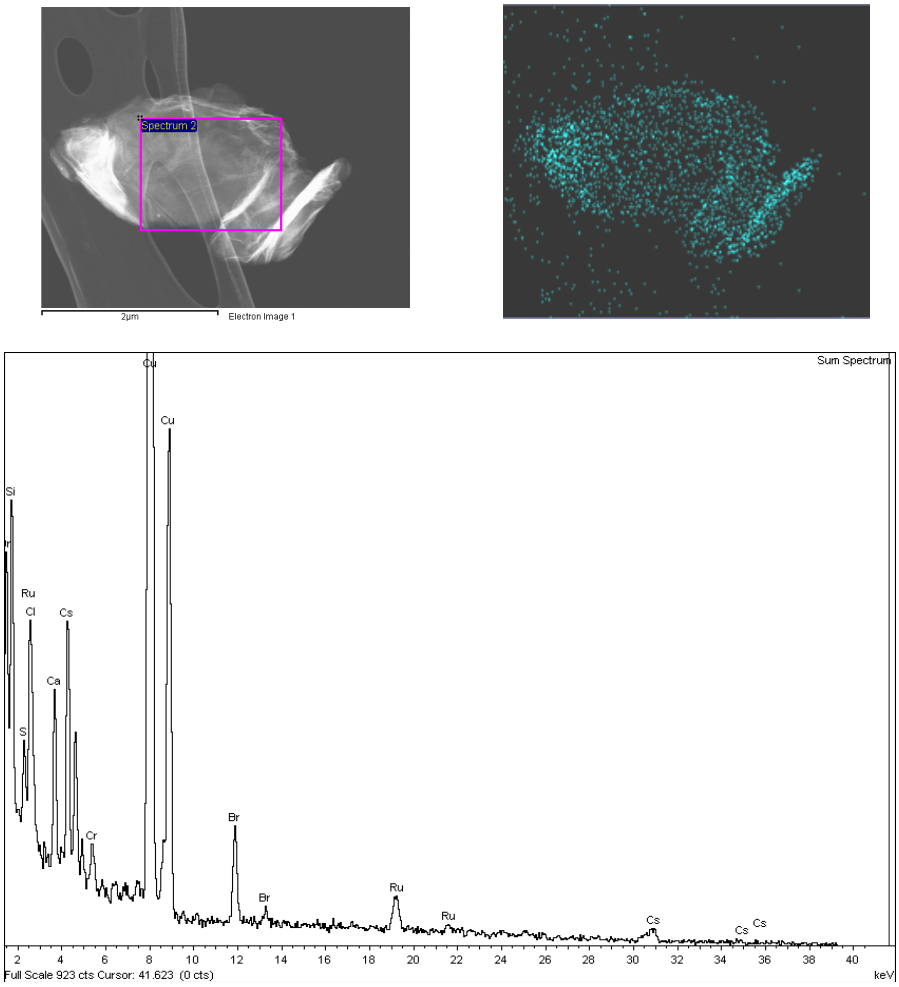

Figure S11. STEM and EDS elemental mapping images (top) and EDS spectrum (bottom) of Ant-Ru-rGO (**5**) showing the homogeneous distribution of ruthenium on the surface after ten catalytic runs.

8. Time-conversion profile for the dehydrogenation of (*p*-trifluoromethyl)benzyl alcohol

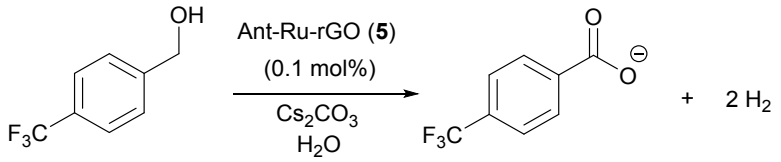

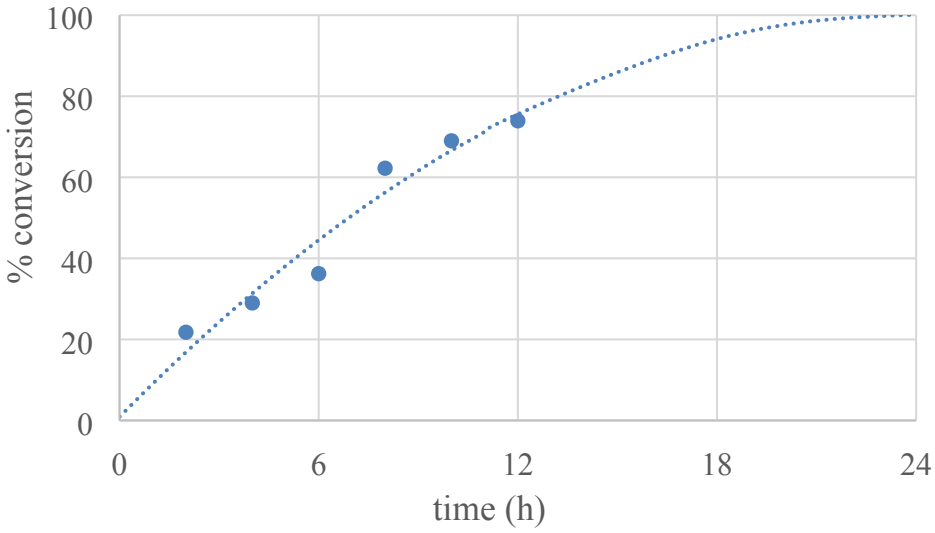

Figure S12. Time-conversion profile for the dehydrogenation of (*p*-trifluoromethyl) benzyl alcohol. Reaction conditions: Substrate (1 eq), Cs_2CO_3 (1 eq), Ant-Ru-rGO (**5**) 0.1 mol %, 10 mL of water at 100 °C. Conversions determined by GC analysis using anisole as external standard.

9. Mechanism

9.1 Nuclear Magnetic Resonance

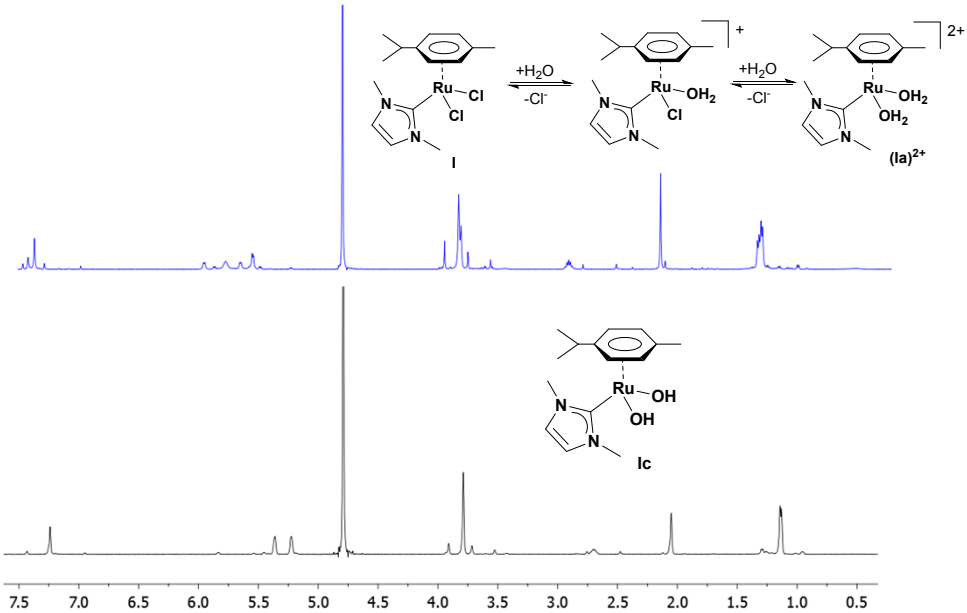

Figure S13. ^{1}H NMR of ruthenium complex **I** in D_2O. Presence of multiple sets and significant line broadening at room temperature is indicative of the co-existence of several species in equilibrium. Bottom: ^{1}H NMR of **I** in D_2O after the addition of a strong base. One set of signals corresponding to the complex (**Ic**).

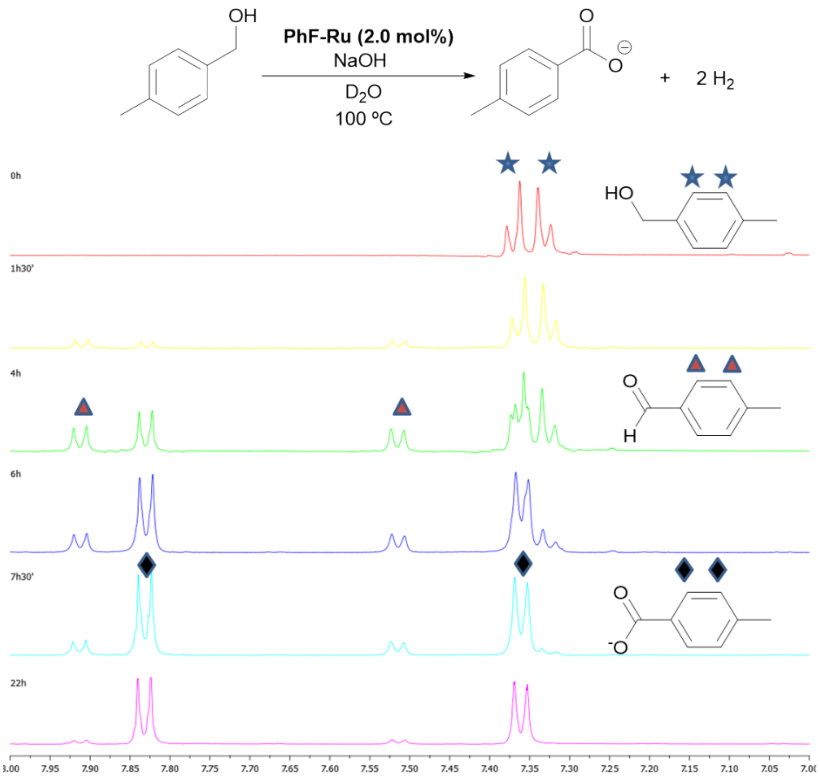

Figure S14. Monitoring of the reaction by ^{1}H NMR using D_2O showing the formation of the intermediate *p*-methylbenzaldehyde. Reaction conditions: *p*-methylbenzyl alcohol (0.5 mmol), NaOH (1 eq), catalyst (0.1 mol %), 4 mL of D_2O at 100 °C

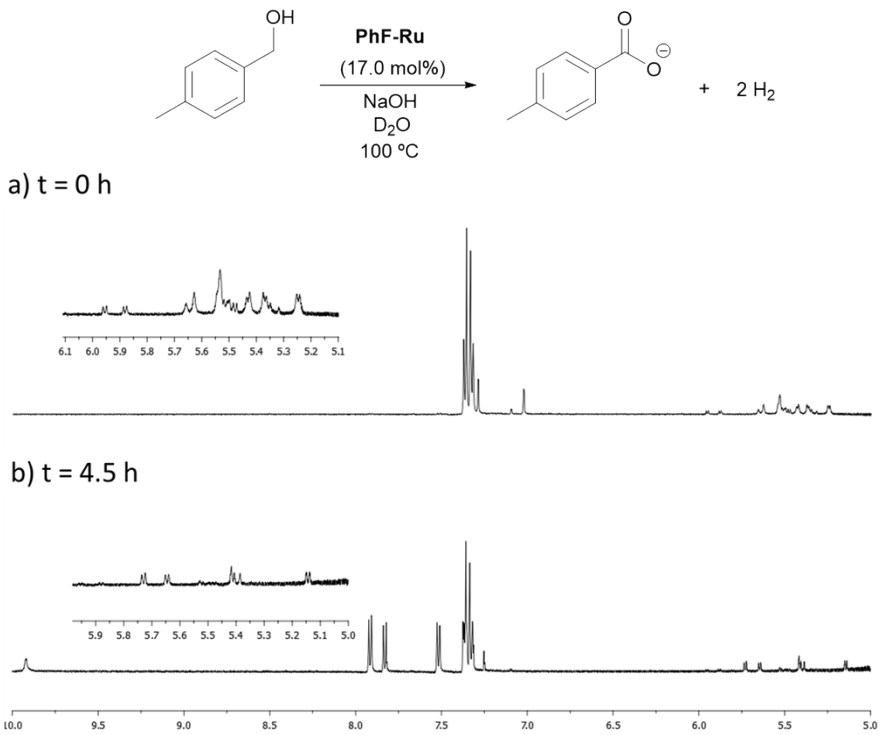

Figure S15. Monitoring of the reaction by ^{1}H NMR using D_2O at high catalyst loading. Reaction conditions: *p*-methylbenzyl alcohol (0.1 mmol), NaOH (1 eq), catalyst (17.0 mol %), 5 mL of D_2O

at 100 °C. a) t = 0, shows the presence of multiple signals corresponding to the *p*-cymene ligand in the region of 5.0 to 6.0 ppm indicative of the co-existence of several species in equilibrium similar to the experiment described in Figure S13. b) t = 4.5 h, at ca. 40 % conversion, the signals corresponding to the *p*-cymene are still observed, indicating that the arene is not lost during the catalysis.

9.2 Electrospray ionization mass spectrometry (ESI-MS)

Mechanistic insights using Electrospray ionization mass spectrometry (ESI-MS) were obtained using compound PhF-Ru (**1**) as a representative member of the series of the catalysts investigated herein. Detailed insights into the aqueous chemical speciation of PhF-Ru (**1**) were gathered from single-stage ESI-MS. Typically, an aqueous solution of compound PhF (**1**) was stirred and aliquots were extracted at spaced time intervals, diluted with water to a final concentration of 5 x 10^{-5} M and directly introduced to the mass spectrometer. The ESI mass spectrum of aqueous solutions of neutral PhF-Ru (**1**) is dominated by species lacking chlorine ligands as judged by their m/z values as well as their characteristic isotopic pattern. Two major peaks at m/z = 249.0 and m/z = 515.0 are observed that formally correspond to [PhF-Ru (**1**) – 2Cl]$^{2+}$ and [PhF-Ru (**1**) – 2Cl + OH]$^{+}$. As the pH is raised by the addition of NaOH, ionic species featuring Ru-OH functional groups become more intense. As illustrated in figure S15, the [PhF-Ru (**1**) – Cl + OH]$^{+}$ and [PhF-Ru (**1**) – 2Cl + 2OH + Na]$^{+}$ cations (this latter is the base peak) were observed in their respective ESI mass spectra at pH values 8 and 12, respectively. Note that different ionization mechanisms are potentially operative and/or competitive in the presence of the Na^{+} cationizing agent used to reach the basic media. To circumvent the effect of the cationizing agent, we performed the ESI-MS experiments by keeping the alkali content constant during the dilution step. For example, we observe that the identity of the species detected in the ESI mass spectra of compound PhF-Ru (**1**) in H_2O and H_2O with $NaBF_4$ was identical, thus confirming that the formation of the dihydroxo species, namely [PhF-Ru (**1**) – 2Cl + 2OH + Na]$^{+}$ is due to the basic media rather than the high content of Na^{+}. A plausible aqueous chemical speciation mechanism is depicted in Figure S15 where the species PhF (**1a**)$^{2+}$ with two water molecules is sequentially deprotonated to PhF-Ru (**1b**)$^{+}$ and PhF-Ru (**1c**) as the pH is raised. We note that ligated H_2O molecules in PhF-Ru (**1a**)$^{2+}$ were not detected, and for and PhF-Ru (**1b**)$^{+}$, the attached H_2O molecule was barely observed, most likely because they are loosely bound and are released upon ESI ionization. This is an indication that unsaturated species could also be present in the solution. Overall, the ESI-MS results suggest that i) immediate Ru-Cl chloride cleavage and subsequent water coordination at the vacant site takes place rapidly upon dissolving in PhF-Ru (**1**) in water and ii) as the pH is raised deprotonation of one or the two water molecules takes place.

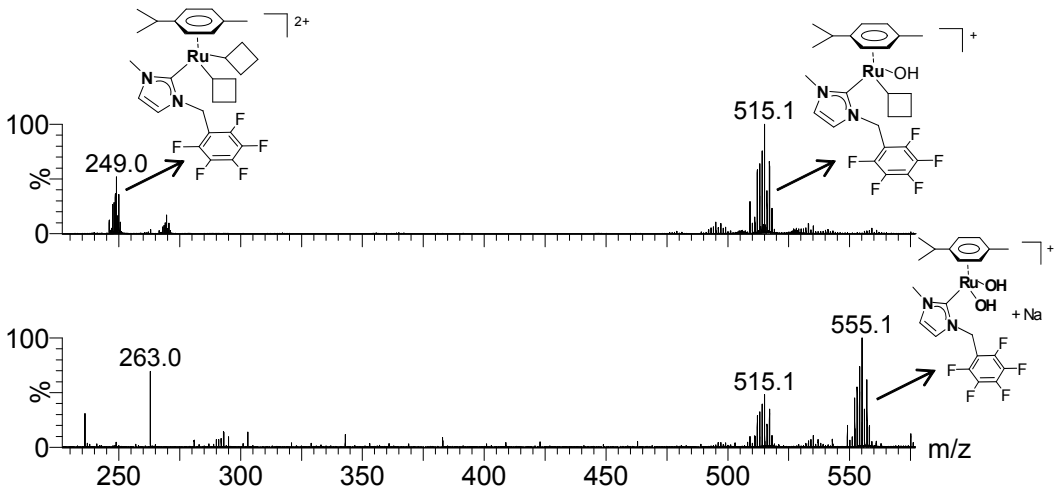

Figure S16. ESI mass spectrum of aqueous solution of PhF-Ru (**1**) at pH 8 and 12, respectively.

When an excess of benzylalcohol was added and the temperature was raised to 100 ^{o}C in the presence of NaOH, the ESI-MS spectra displayed species corresponding to the alkoxide and carboxylate species derived from the benzyl alcohol (Figure S16) as well as signals attributed to hydride species. These experimental evidences are fully consistent with the occurrence of alcohol activation and dehydrogenation. Remarkably, the propensity of the alkoxide [**II** – H_2O]$^+$ species to yield the aldehyde was manifested upon investigating the CID spectrum of the species [**II**-H_2O]$^+$. The CID experiment reveals the exclusive release of aldehyde from the [**II**-H_2O]$^+$ complex concomitant with the formation of Ru hydride species (Figure S17).

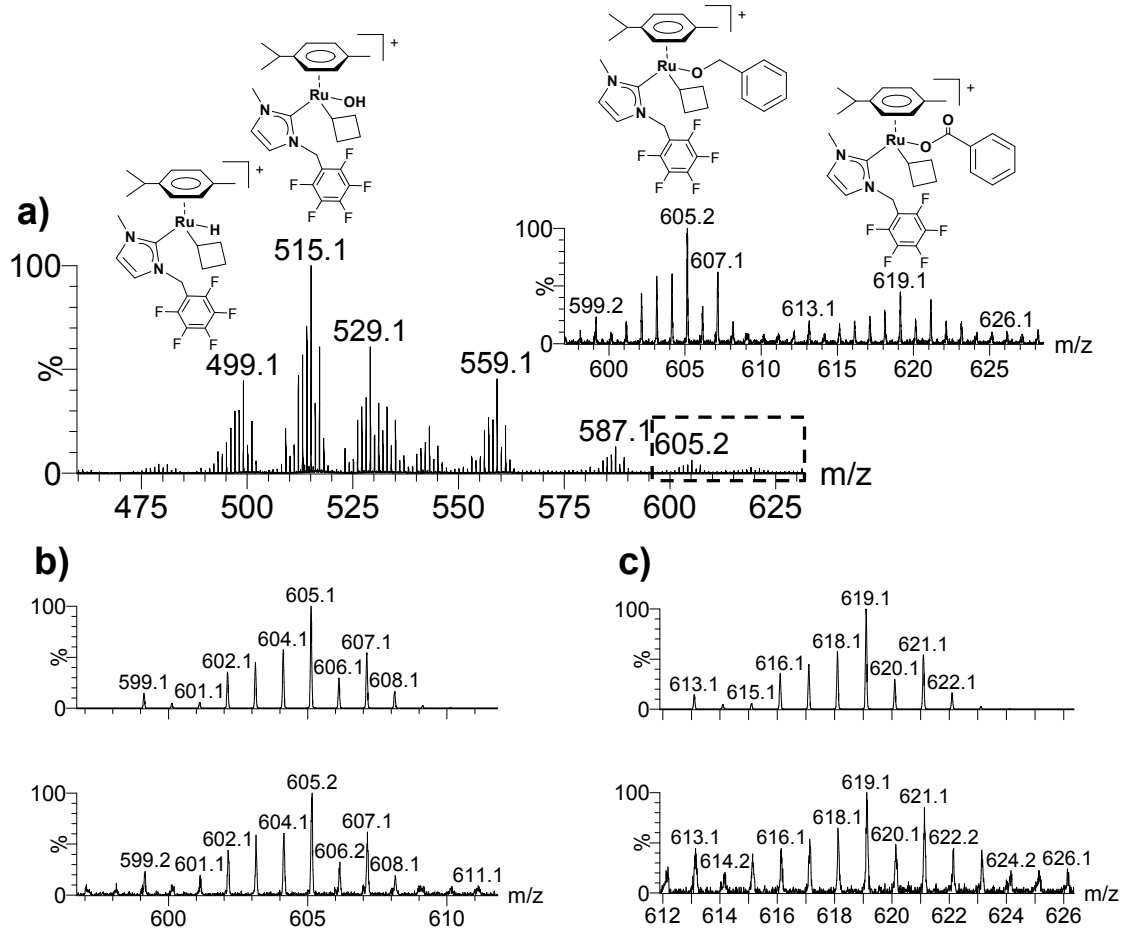

Figure S17. (a) ESI mass spectrum of aqueous solution of PhF-Ru (**1**) in the presence of benzylalcohol under catalytic conditions (schematic drawings of the intermediates featuring hydride, hydroxo, alkoxide and carboxylic functionalities). (b) experimental (top) and simulated (bottom) isotopic pattern of the alkoxide intermediate [**II** – H_2O]$^+$. (c) experimental (top) and simulated (bottom) isotopic pattern of the carboxylic acid intermediate formulated as [(p-cym)(NHC)Ru($PhCO_2$)]$^+$.

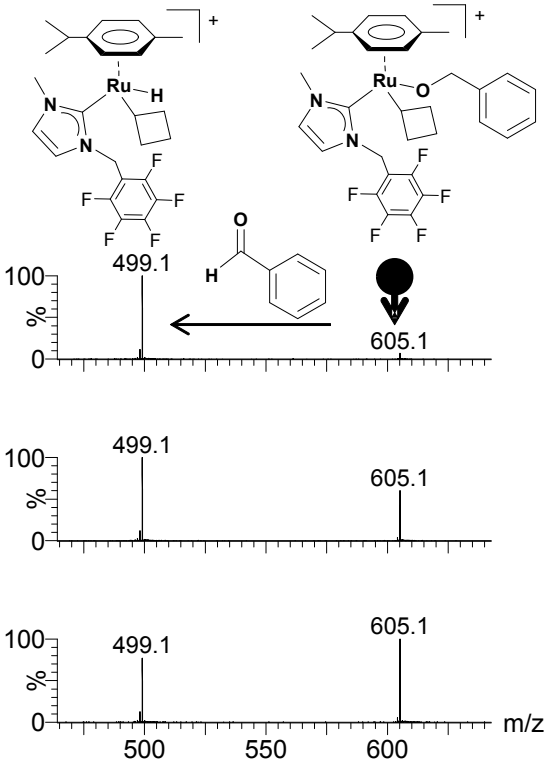

Figure S18. CID mass spectra of the mass-selected alkoxide intermediate [**II** – H_2O]$^+$ at m/z 605.1 at increasing collision energies (Elab = 5 eV (bottom), 10 eV (middle) and 15 eV (top).

9.3 DFT calculations. Computational details

Quantum mechanical calculations were performed with the Gaussian09 package[1] at the DFT/M06 level of theory.[2] SDD basis set and its corresponding effective core potentials (ECPs) were used to describe the Ruthenium atom.[3] An additional set of f-type functions was also added.[4] Carbon, nitrogen, oxygen and hydrogen atoms were described with a 6-31G** basis set.[5,6] Frequency calculations have been performed in order to determine the nature of the stationary points found (no imaginary frequencies for minima, only one imaginary frequency for transition states). Free Gibbs energies in water solution (ε = 78.3553) were calculated by computing the energy in the solvent by means of single-point calculations on the gas-phase optimized geometries with the SMD continuum solvation model,[7] and subsequently applying the following expression:

$$G_{water} = E_{water} + (G_{gas\ phase} - E_{gas\ phase})$$

The DFT optimized structures relevant for the discussion are included in an independent file accessible as supplementary material.

References:

(1) Frisch, M. J.; et al. *Gaussian 09, revision D.01* Gaussian, Inc., Wallingford CT, **2013**.

(2) Zhao, Y.; Truhlar, D. G. *Theor. Chem. Acc.* **2008**, *120*, 215-241.

(3) Andrae, D.; Häussermann, U.; Dolg, M.; Stoll, H.; Preuss, H. *Theor. Chim. Acta* **1990**, *77*, 123-141.

(4) Ehlers, A. W.; Böhme, M.; Dapprich, S.; Gobbi, A.; Höllwarth, A.; Jonas, V.; Köhler, K. F.; Stegmann, R.; Veldkamp, A.; Frenking, G. *Chem. Phys. Lett.* **1993**, *208*, 111-114.

(5) Harihara, P. C.; Pople, J. A. *Theor. Chim. Acta* **1973**, *28*, 213-222.

(6) Francl, M. M.; Pietro, W. J.; Hehre, W. J.; Binkley, J. S.; Gordon, M. S.; Defrees, D. J.; Pople, J. A. *J. Chem. Phys.* **1982**, *77*, 3654-3665.

(7) Marenich, A. V.; Cramer, C. J.; Truhlar, D. G. *J. Phys. Chem. B* **2009**, *113*, 6378-6396.

Complete Gaussian reference:

Gaussian 09, Revision D.01, M. J. Frisch, G. W. Trucks, H. B. Schlegel, G. E. Scuseria, M. A. Robb, J. R. Cheeseman, G. Scalmani, V. Barone, B. Mennucci, G. A. Petersson, H. Nakatsuji, M. Caricato, X. Li, H. P. Hratchian, A. F. Izmaylov, J. Bloino, G. Zheng, J. L. Sonnenberg, M. Hada, M. Ehara, K. Toyota, R. Fukuda, J. Hasegawa, M. Ishida, T. Nakajima, Y. Honda, O. Kitao, H. Nakai, T. Vreven, J. A. Montgomery, Jr., J. E. Peralta, F. Ogliaro, M. Bearpark, J. J. Heyd, E. Brothers, K. N. Kudin, V. N. Staroverov, T. Keith, R. Kobayashi, J. Normand, K. Raghavachari, A. Rendell, J. C.

Burant, S. S. Iyengar, J. Tomasi, M. Cossi, N. Rega, J. M. Millam, M. Klene, J. E. Knox, J. B. Cross, V. Bakken, C. Adamo, J. Jaramillo, R. Gomperts, R. E. Stratmann, O. Yazyev, A. J. Austin, R. Cammi, C. Pomelli, J. W. Ochterski, R. L. Martin, K. Morokuma, V. G. Zakrzewski, G. A. Voth, P. Salvador, J. J. Dannenberg, S. Dapprich, A. D. Daniels, O. Farkas, J. B. Foresman, J. V. Ortiz, J. Cioslowski, and D. J. Fox, Gaussian, Inc., Wallingford CT, 2013.